# Investigating quenching mechanisms in $CO_2$ mixtures by spatially resolved tunable diode laser absorption spectroscopy of metastable atoms in an atmospheric pressure plasma Jet

**Bachelor Thesis**

in the

Degree Program

"Bachelor of Science"

in Physics

at the Faculty of Physics and Astronomy
of the Ruhr-Universität Bochum

by

Amira Aouicha Nouira

from

(Tunisia)

Bochum, 2025

**Abstract**

This study examines how argon metastable atoms are quenched in plasmas operating at atmospheric pressure with small amounts of $CO_2$. The focus is on the metastable states He $(2^3S_1)$ and Ar $(^3P_2)$. Their densities were measured with high spatial resolution using tunable diode laser absorption spectroscopy (TDLAS). All experiments were carried out with the COST reference microplasma jet, operated at 13.56 MHz, using different gas mixtures of He, Ar, and $CO_2$. The main goal was to understand how the metastable density and its spatial profile change for different argon admixtures, applied powers, and small additions of $CO_2$. This was done to see how $CO_2$ removes energy from the plasma and how this influences the dissociation pathways of $CO_2$.

Measurements did not reveal any significant presence of helium metastable states under the given plasma conditions. This can be explained by the high excitation energy of helium and by the fact that argon dominated the discharge in our conditions. In contrast, argon metastable atoms were clearly detected. Even very small amounts of $CO_2$ caused a strong decrease of the argon metastable density under all conditions. This reduction can be explained by additional energy-loss channels in $CO_2$, such as vibrational and electronic excitation, as well as electron attachment. These processes compete with electron-impact excitation and therefore prevent the formation of a high metastable density. The spatially resolved data also show that $CO_2$ weakens the excitation close to the sheath regions and leads to a flatter profile in the center of the discharge.

Overall, the results indicate that, under the conditions of this study, argon metastable atoms play only a small role in $CO_2$ dissociation. Their density is mainly reduced by quenching and electron losses, not by direct interactions with $CO_2$. These findings give a clearer picture of how $CO_2$ removes energy from the plasma and can help in future work to improve $CO_2$ conversion in atmospheric pressure plasmas.

## Zusammenfassung

In dieser Arbeit wurde untersucht, wie Argon-Metastabilzustände in Plasmen bei Atmosphärendruck durch kleine Mengen an $CO_2$ gequencht werden. Im Mittelpunkt stehen die Metastabilzustände He $(2^3S_1)$ und Ar $(^3P_2)$. Ihre Dichten wurden mit hoher räumlicher Auflösung mittels tunabler Diodenlaser-Absorptionsspektroskopie (TDLAS) gemessen. Alle Experimente wurden mit dem COST-Referenzmikroplasmajet bei 13.56 MHz durchgeführt, unter Verwendung verschiedener Gasgemische aus He, Ar und $CO_2$.

Das Hauptziel bestand darin zu verstehen, wie sich die Metastabilendichte und ihr räumliches Profil bei unterschiedlichen Argonbeimischungen, eingekoppelten Leistungen und kleinen $CO_2$-Zusätzen verändern. Dies wurde getan, um zu untersuchen, wie $CO_2$ Energie aus dem Plasma entzieht und wie dies die Dissoziationswege von $CO_2$ beeinflusst.

Unter den gegebenen Plasmabedingungen konnten keine signifikanten Helium Metastabilzustände nachgewiesen werden. Dies lässt sich durch die hohe Anregungsenergie von Helium sowie dadurch erklären, dass Argon in unseren Bedingungen die Entladung dominierte. Im Gegensatz dazu wurden Argon-Metastabilzustände deutlich detektiert. Bereits sehr kleine Mengen an $CO_2$ führten unter allen Bedingungen zu einer starken Abnahme der Argon-Metastabilendichte. Diese Reduktion lässt sich durch zusätzliche Energieverlustkanäle in $CO_2$ erklären, wie zum Beispiel vibronische und elektronische Anregung sowie Elektronenanlagerung. Diese Prozesse konkurrieren mit der Elektronenstoßanregung und verhindern daher die Bildung einer hohen Metastabilendichte. Die räumlich aufgelösten Daten zeigen zudem, dass $CO_2$ die Anregung in der Nähe der Schichtregionen abschwächt und zu einem flacheren Profil im Zentrum der Entladung führt.

Insgesamt deuten die Ergebnisse darauf hin, dass Argon-Metastabilzustände unter den Bedingungen dieser Studie nur eine geringe Rolle bei der $CO_2$-Dissoziation spielen. Ihre Dichte wird hauptsächlich durch Quenching und Elektronenverluste reduziert und nicht durch direkte Wechselwirkungen mit $CO_2$. Diese Erkenntnisse ermöglichen ein klareres Verständnis darüber, wie $CO_2$ Energie aus dem Plasma entzieht, und können in zukünftigen Arbeiten dazu beitragen, die $CO_2$-Konversion in Atmosphärendruckplasmen zu verbessern.

# Contents


**1 Introduction** **2**

**2 Fundamentals** **5**
2.1 Characterization of Plasmas . . . . . 5
2.1.1 Heating Mechanisms . . . . . 7
2.2 Metastable States of Helium and Argon . . . . . 8
2.2.1 Roles of Metastable atoms in Plasma Processes . . . . . 9
2.3 Absorption Spectroscopy . . . . . 12
2.3.1 Line Broadening in Absorption Spectroscopy . . . . . 13

**3 Experimental Setup and Calibration** **16**
3.1 Plasma Source . . . . . 16
3.2 Gas Supply System . . . . . 18
3.3 The Laser and Optical System . . . . . 18
3.4 Positioning System . . . . . 20
3.5 Optical Components and Beam Conditioning . . . . . 20
3.5.1 Laser Diodes and Optical Configuration . . . . . 20
3.5.2 Calibration . . . . . 21

**4 Measurements** **25**
4.1 Measurements Challenges and Potential Errors . . . . . 25
4.2 Analysis of Ar Metastable Density with Gas Mixture Variations . . . . . 28
4.2.1 Argon variation with 0.0 and 0.2 sccm of $CO_2$ . . . . . 29
4.3 Power Variation . . . . . 32
4.3.1 Spatial Distribution of Ar Metastable Density . . . . . 33
4.3.2 Spatial Distribution with $CO_2$ Variation . . . . . 36

**5 Conclusion** **38**
5.1 Limitations and Future Perspectives . . . . . 39

**Bibliography** **40**

# 1 Introduction

The dissociation of carbon dioxide ($CO_2$) in non-equilibrium plasmas has become an important research topic in recent years. This process offers a promising method to convert $CO_2$ into useful products, support carbon reuse, synthesize fuels, and reduce greenhouse gases [1, 2, 3].

Atmospheric pressure plasmas, especially those operated with radio-frequency (RF) power, have very high electron densities while the gas itself stays relatively cold. This allows controlled excitation and dissociation of molecules without causing strong heating of the gas. In such plasmas, metastable species act as internal energy reservoirs and participate in key energy transfer processes such as Penning ionization, vibrational excitation, and collisional quenching [4, 5, 6].

Among these, the metastable states of He ($2\,^3S_1$) and Ar ($3\,^3P_2$) are especially important since their excitation energies (19.82 eV and 11.55 eV, respectively) exceed the dissociation threshold of $CO_2$. This makes Penning-type reactions energetically possible. However, the efficiency of these processes is strongly reduced by quenching reactions with $CO_2$ and other molecules. This reactions can significantly reduce metastable lifetimes and alter the local plasma chemistry [5, 7].

Recent investigations have demonstrated that adding argon to helium based non equilibrium plasmas can enhance $CO_2$ conversion performance. In an atmospheric pressure RF plasma jet, Stewig et al. [8] observed that replacing helium with argon as a carrier gas significantly increases the dissociation efficiency, from about 45% in pure helium to nearly 85% in pure argon discharges, this is shown in Figure 1.1. This improvement was attributed to the lower excitation energy of argon metastable atoms and the lower ionization energy of argon atoms, which allows for a higher electron density in Ar plasmas compared to He. This, in turn, leads to more efficient energy transfer to $CO_2$ molecules. Nevertheless, the overall conversion efficiency remains limited by the strong quenching of metastable and vibrational excited states in plasmas with added $CO_2$ [8, 9]. Understanding these quenching mechanisms is therefore important for improving the energy efficiency of $CO_2$ plasmas. In this work, spatially resolved tunable diode laser absorption spectroscopy (TDLAS) was used to investigate the local quenching behavior of metastable atoms by measuring the spatially resolved densities of Ar ($^3P_2$) along the plasma jet under varying $CO_2$ admixtures.

The applied plasma power also strongly influences the $CO_2$ conversion, as shown in Figure 1.1. At low power levels, the conversion remains generally low, but it increases noticeably when the power is raised. For instance, in a pure helium plasma, the $CO_2$ conversion at approximately 4.5 W is about 45% compared to about 12% at 1 W. When 10% argon is added, the $CO_2$ conversion also increases with power, reaching values around 70 to 75% at 4.5 W, which is noticeably higher than in pure helium at the same power.

These results show that both the amount of argon and the applied plasma power strongly influence the $CO_2$ conversion efficiency. This demonstrates the importance of controlling discharge conditions to maintain favorable metastable production while minimizing their loss through quenching [8].

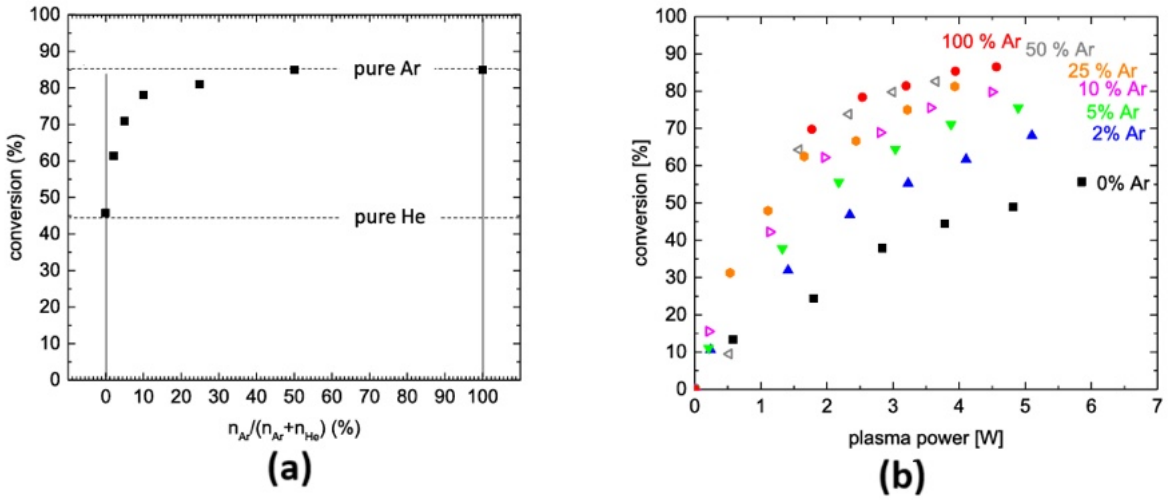


Figure 1.1: $CO_2$ conversion in a helium atmospheric pressure RF plasma from Stewig et al. [8]. (a) Conversion as a function of argon admixture showing the increase from pure He to pure Ar. (b) Conversion as a function of applied plasma power for several Ar admixtures (0-100% Ar).

To better understand the role of metastable atoms in the dissociation of $CO_2$, it is first necessary to examine the behavior of helium and argon in a plasma without the presence of $CO_2$. A similar investigation was carried out in a previous master's thesis [10] related to this topic. That study examined the spatial distribution and density of metastable species for varying argon admixtures (up to 1%) under different power conditions.

This earlier work will be referenced in several sections of the present thesis, as the plasma source and experimental setup were largely the same. Both studies use the COST reference jet design described by Golda *et al.* [11]. This standardized atmospheric pressure plasma source was developed within the COST framework to enable different research groups to compare their results under identical discharge conditions.

The main difference between the setup used in this work and that of the master thesis lies in a few technical improvements implemented here, such as the installation of a pump to minimize impurity levels in the system.

In this thesis, we extend the investigation to study how the presence of $CO_2$ alters not only the absolute metastable densities but also their spatial distribution within the discharge. In particular, we focus on revealing how quenching processes influence the excitation profile of metastable argon across the plasma gap, as measured by spatially resolved tunable diode laser absorption spectroscopy (TDLAS). While global density values provide useful information, quenching effects are not uniform throughout the plasma. Regions near the sheath and the bulk can differ significantly in their metastable dynamics due to localized electron energy and transport. Therefore, spatially resolved measurements are essential to uncover where quenching is most pronounced. Previous optical diagnostic studies on atmospheric pressure plasma jets have demonstrated strong spatial

gradients in metastable densities and emission intensities [7].

One main advantage of atmospheric pressure plasmas is that they do not require a vacuum system, which makes it possible to treat materials that cannot be placed in a vacuum. This includes, for example, polymers and soft plastics that can deform under reduced pressure, liquid samples that would evaporate and biological or organic substrates that cannot tolerate vacuum environments. Another benefit is the low gas temperature of RF plasmas, which allows the treatment of temperature sensitive materials such as biological tissue or human skin [6].

Tunable diode laser absorption spectroscopy (TDLAS) was used to measure the spatial distribution of helium and argon metastable atoms in the plasma jet and to see how their densities decrease when $CO_2$ causes quenching. In this method, metastable atoms are resonantly excited by the light of a tunable laser diode. These lasers can scan over individual transition lines by adjusting the frequency within the GHz range, allowing highly selective and non-intrusive detection [5]. From the amount of light absorbed, the density of metastable species can be determined. Since only relative absorption is used, no calibration is needed. Another advantage of this method is its high sensitivity, because the coherent laser makes it possible to detect very small amounts of metastable atoms. Both helium and argon metastable profiles are measured using two separate lasers tuned to their respective transitions. By scanning the laser beam at different vertical positions through the jet, the technique provides spatially resolved metastable density profiles, which makes it possible to observe how increasing $CO_2$ admixture affects metastable quenching and their spatial distribution.

# 2 Fundamentals

## 2.1 Characterization of Plasmas

Plasma is commonly referred to as a partially or fully ionized gas composed of ions, electrons, and neutral species that exhibit collective interactions. This thesis investigates discharges generated at atmospheric pressure using radio-frequency (RF) excitation. In order to understand the importance of RF excitation in this context, it is useful to first consider the simpler case of direct current (DC) discharges [12].

DC discharges provide the fundamental framework for plasma ignition through *Townsend's theory of gas breakdown*. The mechanism is relatively simple: an electric field is applied across two electrodes with a neutral gas in between. To start the discharge, a few free electrons are necessary. These electrons can come from natural sources such as photo-ionization or cosmic radiation. These electrons are accelerated by the electric field and gain enough energy to ionize neutral gas atoms during collisions. This initiates an *electron avalanche*, where each ionization event produces additional free electrons, leading to exponential growth in the charged-particle density.

The electrons then move toward the anode and create an electric current. At the anode, this current is described by the following equation:

$$I = I_0 \cdot \exp(\alpha d) \tag{2.1}$$

where $I_0$ is the initial current at the cathode and $d$ is the distance between the electrodes. The **first Townsend coefficient** $\alpha$ represents the number of ionizing collisions per unit length. A higher value of $\alpha$ increases the probability of sustaining this avalanche effect.

To keep the plasma running, new electrons must be continuously created. This happens when the positive ions from the avalanche hit the cathode and cause it to release secondary electrons. This effect is described by the **second Townsend coefficient** $\gamma$, which defines how many electrons are emitted per incoming ion [13, 14]. To sustain the plasma discharge, every electron must generate at least one new electron. This is described by the *Townsend breakdown criterion*:

$$\gamma \left(e^{\alpha d} - 1\right) = 1 \tag{2.2}$$

where $d$ is the distance between the electrodes.

The coefficients $\alpha$ and $\gamma$ describe the microscopic mechanisms of ionization and electron multiplication. The macroscopic outcome of these processes is described by *Paschen's Law*. It relates the breakdown voltage $V$ to the product $pd$ (gas pressure times electrode gap distance):

$$V = \frac{B \cdot pd}{\ln(A \cdot pd) - \ln\left[\ln\left(1 + \frac{1}{\gamma}\right)\right]} \tag{2.3}$$

where $A$ and $B$ are gas and electrodes material specific constants. This equation describes the *Paschen curve*, which plots the breakdown voltage $V$ as a function of the product $pd$ [14].

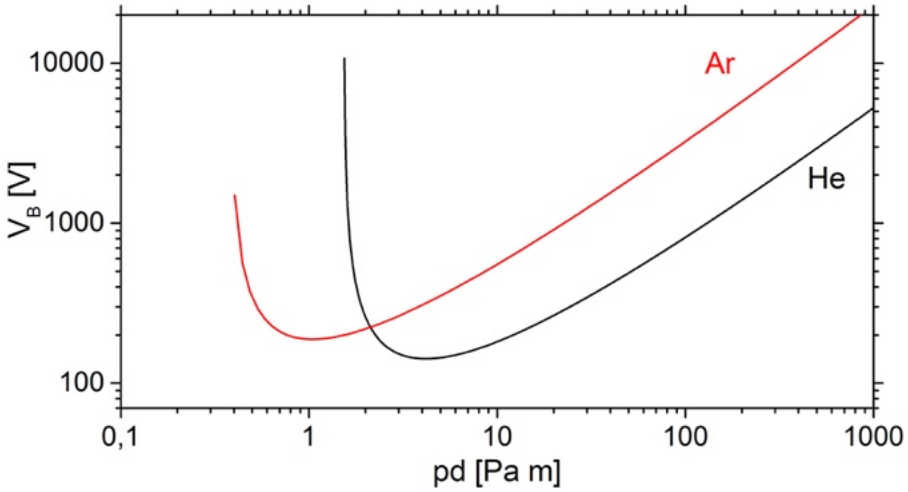


Figure 2.1: Paschen curve illustrating the breakdown voltage as a function of the pressure-distance product $pd$ from [15].

When $pd$ is large, a higher voltage is needed to ignite the plasma. At high pressure the gas density is high, this translates to a short mean free path for the electrons and therefore a high collision possibility. However, they also lose energy quickly. A strong electric field (high voltage) is needed to give electrons enough energy to ionize atoms before they lose energy. For small values of $pd$, the mean free path becomes long, but the electrons have fewer chances to collide before they reach the anode. If the gap is too small, the electrons cannot gain enough energy from the electric field to ionize the gas, even though their mean free path is long. Because of this, there is an optimal $pd$ value where the breakdown voltage reaches its minimum [14].

In atmospheric pressure plasmas, many collisions take place, which leads to a high electron density. These electrons can weaken the external electric field, a process known as plasma shielding. If the electric field created by the electrons becomes as strong as the applied field, a streamer can form. Once the streamer reaches the opposite electrode, it forms a low-resistance path. This allows a sudden rise in current, called an arc discharge, which can seriously damage the electrodes [16].

To avoid the formation of arcs and streamers at atmospheric pressure, different methods are used to keep the discharge stable. In dielectric barrier discharges, a dielectric layer on the electrodes limits the current and suppresses arcing. In our case, the plasma is driven at radio-frequency (RF), so the electric field reverses before a streamer can reach the electrode. This prevents the transition to an arc. A microplasma source also helps to keep the discharge stable. Because the electrodes are very close to each other, a high electric field can be created in a small area without creating long streamer channels [16].

The source of the plasma used for this work is the COST-Jet. It is characterized by a small cross-sectional area between the electrodes. This compact geometry allows plasma ignition at atmospheric pressure with low breakdown voltage [11]. The COST-Jet operates with an RF discharge. This means that the ignition and heating mechanisms

are a bit different from those in a DC discharge. In RF plasmas, the electric field changes direction constantly. In the case without collisions, the electrons would just follow the field back and forth without gaining energy overall. However, because the electrons collide often with neutral gas atoms, they become out of phase with the electric field. This causes them to gain energy on average. For ignition to happen, each electron needs to produce at least one new electron before it is lost to the wall through diffusion. The ignition curve in RF plasmas is similar to that in the DC case, but it requires a lower voltage. This behavior can be illustrated using the RF and DC breakdown measurements reported by Woodruff et al. [17]. Figure 2.2 shows that, for the same *pd* product, the RF breakdown voltage in argon, helium, and xenon follows the same Paschen like curve as the DC case, but with lower ignition voltages. However, if the voltage becomes too high, the plasma can shift into a constricted or unstable mode, just as in DC discharges [18].

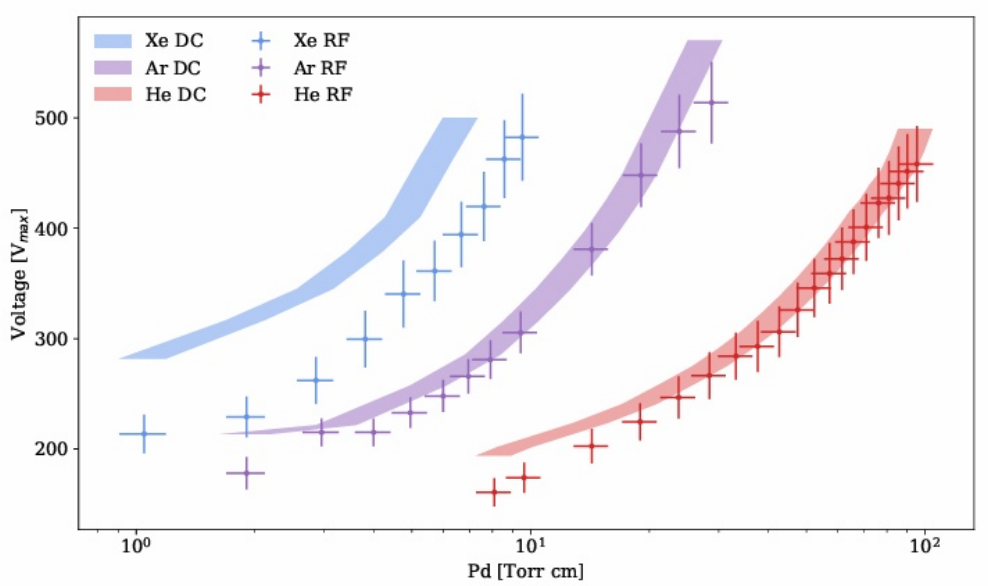


Figure 2.2: Comparison of RF and DC breakdown voltages in He, Ar, and Xe as a function of the *pd* product, adapted from Woodruff et al. [17].

### 2.1.1 Heating Mechanisms

When a voltage is applied to a gas, how the plasma is heated depends on the strength of the voltage and on the type of gas. In atmospheric pressure RF plasmas, especially when using helium or argon, two main heating modes can be seen.

#### Ohmic Mode (Ω-mode)

Ohmic mode often appears in helium plasmas when the applied voltage is low and the pressure is atmospheric. Under these conditions, it usually dominates in helium but is less pronounced in pure argon. In this mode, electrons absorb energy from the oscillating RF field, which can reach the bulk. This is possible because, at atmospheric pressure, the frequent electron–neutral collisions give the plasma a high effective resistivity. Heating is mainly due to ohmic (Joule) heating, where electrons transfer the absorbed energy to the gas through collisions. This helps to sustain the discharge. Ionization is driven by direct

electron-impact ionization, and in helium it is further supported by stepwise processes involving metastable atoms. The electric field in the bulk varies over the RF cycle as the sheaths expand and collapse, giving the plasma a diffuse and uniform appearance. In argon, maintaining Ohmic mode is more difficult, so the discharge tends to shift to other heating modes at higher voltages. [19, 20].

#### Penning Mode ($\gamma$-like Mode)

When the applied voltage becomes higher, the behavior of the discharge changes and the sheaths near the electrodes start to control most of the energy transfer. In this situation, the plasma moves into a regime that is often called a "$\gamma$-like mode." It is similar to the classical gamma mode known from DC plasmas, but at atmospheric pressure it behaves differently.

In this regime, the creation of secondary electrons becomes much stronger. The important difference from low-pressure discharges is that these electrons are not mainly produced when ions hit the electrode surface. Instead, they are often created inside the plasma volume, especially close to the sheath regions.

Ionization in this mode is supported by two processes that work together. One is Penning ionization, where metastable atoms such as He* or Ar* transfer their internal energy to nearby molecules like $CO_2$ or to other argon atoms, allowing ionization without direct electron impact. The other is stepwise ionization, where atoms are first excited into long-lived metastable states during collisions and are then ionized later through additional, lower-energy collisions.

The electrons that are produced through Penning processes start with low kinetic energy, but they gain energy very quickly. This happens through collisional (Ohmic) heating and also through stochastic interactions with the oscillating electric fields in the sheath. Together, these effects help to keep the discharge stable at higher voltages [21].

## 2.2 Metastable States of Helium and Argon

In non-equilibrium plasmas, some excited atomic or molecular states, called metastable states, play an important role in storing and transferring energy. They are described as "metastable" because transitions back to lower energy levels are forbidden or very unlikely due to quantum mechanical rules, such as parity or spin conservation. For this reason, they can exist for a long time, from microseconds up to milliseconds, depending on the pressure and the plasma conditions [22, 23].

At atmospheric pressure, the electron density is high and collisions happen very often. Because of their long lifetimes, metastable atoms can accumulate and reach high concentrations. In microplasmas, for example, their densities can reach $10^9$–$10^{11}$ cm$^{-3}$ as reported in [24]. Such high densities show how strongly metastable atoms can influence the plasma chemistry and the overall energy balance.

Metastable atoms are mainly lost via collisional processes. They can be quenched by collisions with ground state atoms or molecules (two- or three-body quenching), or removed via "pooling" reactions, where two metastable atoms collide and ionize one of them. In noble gas discharges, modeling studies show that metastable losses are dominated by pooling and quenching reactions, such as:

$$\mathrm{Ar}^* + \mathrm{Ar}^* \rightarrow \mathrm{Ar}^+ + e^- + \mathrm{Ar}. \tag{2.4}$$

Super elastic electron collisions, in which a metastable transfers its internal energy to an electron ($Ar^* + e^- \rightarrow Ar + e'^-$), are generally much weaker for typical metastable atoms in gas discharges [25].

The focus of this study is on the $2^3S_1$ level of helium, located approximately 19.5 eV above the ground state. Due to its forbidden decay to the singlet ground state ($1\,^1S_0$), it is remarkably stable under plasma conditions. However, the $2^3S_1$ state can be optically excited to the higher triplet levels $2\,^3P_J$. This results in observable spectral lines with fine structure:

- $2\,^3S_1 \rightarrow 2\,^3P_0$ at 1083.025 nm
- $2\,^3S_1 \rightarrow 2\,^3P_1$ at 1083.034 nm

For argon, the metastable state of interest is the $^3P_2$ level in LS-coupling notation, also known as $1s_5$ in Paschen notation. Its excitation energy is about 11.55 eV. The transition $1s_5 \rightarrow 2p_9$ corresponds to a spectral line at 811.531 nm [26].

### 2.2.1 Roles of Metastable atoms in Plasma Processes

Metastable atoms play an important role in various plasma processes. Figure 2.3 helps to understand this by showing the energy of the helium and argon metastable states compared with the dissociation and ionization thresholds of species such as $N_2$, $O_2$, $H_2O$, or $CO_2$. This can explain why metastable atoms strongly influence the plasma chemistry. In our study, we are mainly interested in the processes that involve $CO_2$ in the plasma. The figure makes clear that both He $(2^3S_1)$ and Ar $(^3P_2)$ have much higher energies than the levels needed to break or ionize a $CO_2$ molecule. This means that metastable atoms can transfer their internal energy very easily to $CO_2$, which allows processes like Penning ionization or Penning dissociation to happen.

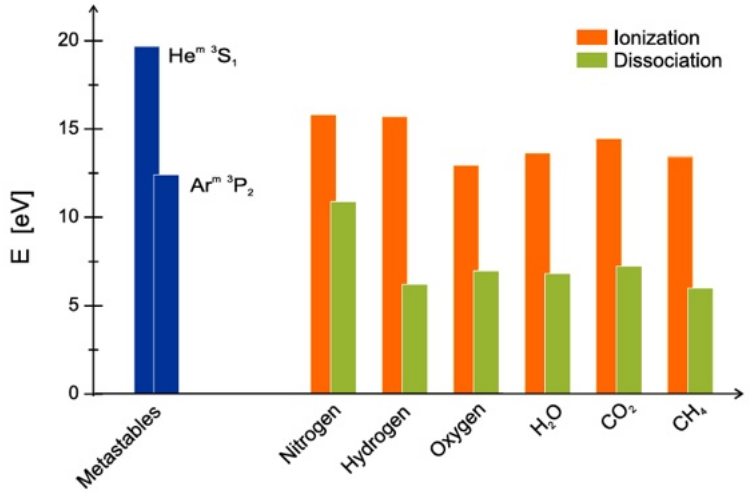


Figure 2.3: Energy levels of the He $(2^3S_1)$ and Ar $(^3P_2)$ metastable states compared with the ionization and dissociation thresholds of common atoms and molecules that are often used as admixtures in plasma chemical processes [27]

### Penning ionization

In Penning ionization, a metastable atom transfers its energy to a neutral atom or molecule when they collide. At atmospheric pressure this process becomes very effective because collisions happen very often. It increases the ionization efficiency and helps to maintain the plasma [14]. In this reaction, a metastable atom ($A^*$) hits a target molecule or atom (M) and transfers its internal energy to ionize it:

$$A^* + M \rightarrow A + M^+ + e^-. \tag{2.5}$$

For example, helium metastable atoms in the $2\,^3S$ state, located at approximately 19.8 eV above the ground state, can ionize nitrogen and oxygen molecules, whose ionization potentials are 15.6 eV and 12.1 eV, respectively.

This process effectively converts the stored metastable energy into free electrons and ions, providing an additional ionization pathway in the discharge. Kassayová *et al.* describe Penning ionization as "an important atomic collision process," where the metastable atom transfers its excitation energy to another species, resulting in ionization [28].

In atmospheric pressure helium plasmas, Penning ionization by $He^*$ is known to be a dominant source of $N_2^+$ and $O_2^+$ ions. This influences the plasma chemistry and helps sustain the discharge. In his PhD thesis, Niermann explained that even very small amounts of impurities, such as only a few ppm of nitrogen or oxygen, can make Penning ionization the dominant source of electron production. This happens because the helium metastable states have a high internal energy and can easily ionize these molecules. This can affect how the plasma forms and how long it remains stable [27]. In the context of our study, an example of an equation involves a helium metastable atom colliding with a carbon dioxide molecule:

$$He^* + CO_2 \longrightarrow He + {CO_2}^+ + e^- \tag{2.6}$$

### Energy Reservoir and Stepwise Ionization

Metastable atoms serve as important energy reservoirs in the plasma. They store electronic energy that can be released later in secondary reactions. One important process supported by metastable atoms is *stepwise ionization*. In this case, an electron first excites an atom into a metastable state. Later, another collision—usually one that requires less energy—can ionize this excited atom. Because of this two-step path, the plasma needs less energy to ionize atoms compared to ionizing them directly from the ground state.

For example, argon can be ionized in two steps: first an atom is excited into a metastable state, and then another electron can ionize it. Because metastable atoms live long enough to accumulate in the discharge, they can clearly increase the total ionization rate. Niermann *et al.* report that these excited states act as major carriers of energy in rare gas plasmas and play an important role in the excitation and ionization processes [24].

In this work we are specifically interested in the energy transfer to $CO_2$. Metastable atoms such as $He^*$ ($2\,^3S_1$, 19.82 eV) and $Ar^*$ ($1s_5$, 11.55 eV) have enough energy to excite or dissociate $CO_2$, whose excitation thresholds range from 3 to 5 eV.

Adding carbon dioxide ($CO_2$) to a He-Ar plasma has a significant impact on the overall energy balance. $CO_2$ is a polyatomic molecule with many vibrational and rotational modes that can efficiently absorb electron energy [9]. As a result, processes that depend on high-energy electrons, such as metastable formation and argon ionization, become less effective [14].

Energy transfer from metastable to $CO_2$ can occur through:

- **Penning Dissociation**

  In this process, an excited atom gives its energy to a neutral molecule.This results in its dissociation into neutral species rather than ionized products. These new species can then take part in other reactions and change the plasma chemistry.

  For example, argon metastable can dissociate carbon dioxide:

  $$Ar^* + CO_2 \longrightarrow Ar + CO + O \tag{2.7}$$

  This reaction breaks the C=O bond in $CO_2$, producing carbon monoxide and atomic oxygen. Similarly, helium metastable atoms can cause the same dissociation.

  The products formed in these reactions are highly reactive. They can help create species such as ozone ($O_3$) or take part in surface oxidation processes. These Penning-related dissociation reactions are also an important loss mechanism for metastable atoms, because collisions with molecules quickly quench their energy and remove them from the metastable population [4, 27].

  A less prominent example of energy transfer to $CO_2$ examined in this study is:

- **Vibrational Excitation**

  In addition to Penning dissociation, carbon dioxide can also be dissociated through vibrational excitation. In this mechanism, electrons or metastable species transfer energy to $CO_2$ and excite its vibrational levels, especially the asymmetric stretch mode. When the molecule reaches high vibrational levels, the states become very close to each other and form an almost continuous range. At this point, the $CO_2$ molecule becomes unstable and dissociates into CO and O without the need for electronic excitation. This process is especially important in non-equilibrium plasmas, where low-energy electrons can efficiently excite vibrational modes [1].

### Influence on Electron Energy Distribution and Plasma Sustainment

Even a very small amount of metastable atoms can significantly modify the electron energy distribution function (EEDF) and influence the overall plasma behavior. Their production requires electrons from the high-energy tail of the EEDF, so each excitation event selectively removes energetic electrons from the distribution. At the same time, metastable atoms can return this stored energy through stepwise or Penning ionization, which introduces additional electrons into the discharge. In this way, metastable atoms regulate the balance between electron loss and electron creation and with that they influence how the discharge develops [27]. Fluid simulations that include metastable kinetics confirm that they "play a major role in the discharge despite the fact that their mole fraction was less than $10^{-5}$ at a pressure of 1 Torr" [25]. At atmospheric pressure, ionization processes that begin from metastable states become even more important, because frequent collisions quickly remove the high-energy electrons. Since metastable atoms provide low threshold, stepwise ionization channels, they can still produce electrons even when direct electron-impact ionization becomes weak. This helps the discharge stay active at lower electric fields or during the later parts of an excitation pulse [27].

### Production of Reactive Species

Metastable atoms play a central role in the generation of reactive species in atmospheric pressure microplasmas. Because they efficiently transfer energy in collisions with impurities such as nitrogen and oxygen. In his Phd, Niermann shows that this effect is in detail for helium and argon metastable states: the Hem($^3S_1$) state, in particular, is highly effective in exciting molecular nitrogen. Through Penning-type energy transfer, Hem can populate the $N_2^+(B^2\Sigma_u^+)$ state, which then emits in the first negative system at 391.4 nm. This pathway demonstrates that metastable atoms act as strong drivers for the formation of energetic nitrogen species in the discharge. Similar behavior is observed for oxygen admixtures. Niermann shows that $O_2$ strongly quenches both Hem and Arm metastable states, as their excitation energies are only a few eV above the ground state of $O_2$. Overall, the dissertation shows that metastable atoms are important intermediaries in exciting molecular species that need high energies. They influence the plasma chemistry much more than what direct electron-impact processes alone could do. These effects explain why molecular emissions, especially from $N_2$ and $N_2^+$, are strongly connected to the metastable behavior in the parallel plate jet [4, 27].

## 2.3 Absorption Spectroscopy

The intensity of a laser beam decreases when it passes through a resonant, absorbing medium. This happens because some of the energy will be transferred to the medium's particles. This occurs when the photon energy ($h\nu$) matches the energy difference ($\Delta E$) between the quantum states. It follows the **Beer-Lambert law**, which relates the transmitted intensity $I(\nu)$ to the initial intensity:

$$I(\nu) = I_0(\nu) \cdot e^{-\alpha(\nu)\cdot L} \tag{2.8}$$

where $\alpha(\nu)$ is the frequency-dependent absorption coefficient, and $L$ is the optical path length through the absorbing medium.

The absorption coefficient is given by:

$$\alpha(\nu) = n_l \cdot k_0 \cdot f_{lu} \cdot \Phi(\nu) \tag{2.9}$$

where:

- $n_l$ is the number density of atoms in the lower (metastable) state,
- $k_0$ is given by:
$$k_0 = \frac{\pi e^2}{m_e c} \tag{2.10}$$
- $f_{lu}$ is the oscillator strength of the transition,
- $\Phi(\nu)$ is the normalized line shape profile,

where $e$ is the elementary charge, $m_e$ is the electron mass and $c$ is the speed of light [29].

By integrating Equation 2.8 across the absorption line, we obtain:

$$\int \ln\left(\frac{I_0(\nu)}{I(\nu)}\right) d\nu = n_l \cdot k_0 \cdot f_{lu} \cdot L \tag{2.11}$$

Solving for $n_l$, the metastable number density:

$$n_l = \frac{1}{k_0 \cdot f_{lu} \cdot L} \int \ln\left(\frac{I_0(\nu)}{I(\nu)}\right) d\nu \tag{2.12}$$

In practical measurements, the raw intensity values are affected by background light, reflections, and detector offsets. To correct for these effects, four different signals are measured:

- $I_{\mathrm{PL}}$ – plasma and laser on,
- $I_{\mathrm{P}}$ – plasma only,
- $I_{\mathrm{L}}$ – laser only,
- $I_{\mathrm{B}}$ – background (both off).

The "plasma on, laser on" measurement indicates how much laser light comes out of the laser source. The "laser off, plasma on" signal provides only the plasma emission. The "laser on, plasma off" gives the reference laser intensity, including reflections and optical losses from the setup, but no plasma emission. The "laser off, plasma off" signal measures the background, such as light from the room.

To get the true transmission ratio, the plasma glow must be subtracted from the laser-plasma signal in the numerator, and the background from the pure laser signal in the denominator:

$$\frac{I_i(\nu)}{I_f(\nu)} = \frac{I_{\mathrm{PL}} - I_{\mathrm{P}}}{I_{\mathrm{L}} - I_{\mathrm{B}}} \tag{2.13}$$

Substituting Equation 2.13 into Equation 2.12 allows an accurate determination of the metastable density [30, 31].

For this analysis we assumed spatial homogeneity along the laser path. In reality, atmospheric pressure plasmas show strong spatial gradients, especially between the sheath and the bulk. However, by using a narrow laser beam, the absorption path can resolve a localized region that is sufficiently homogeneous [24].

### 2.3.1 Line Broadening in Absorption Spectroscopy

In absorption spectroscopy, the observed line shapes are never infinitely narrow. Instead, several physical mechanisms contribute to the broadening of the absorption profile. These effects must be considered when fitting the spectra, because they influence both the line width and the area under the curve, which are essential for determining the density of the absorbing species.

At atmospheric pressure, the dominant broadening mechanism is **collisional broadening, or pressure broadening** [30]. In this regime, frequent collisions disturb the energy levels of the excited states and make the spectral line broader. Two limiting cases

can occur, depending on whether the collisions are slower or faster than spontaneous emission. If the collisions are slower, they shorten the lifetime of the excited state, and because of the Heisenberg uncertainty principle, a shorter lifetime leads to a larger energy uncertainty and a broader line. This impact broadening becomes important only when atoms move quickly and the gas density is low, which is not the case for atmospheric-pressure plasmas such as the COST-Jet. When the collisions are much faster than spontaneous emission, the excited atom experiences continuous perturbations from nearby particles. These interactions include long-range van der Waals forces ($n = 6$), resonance dipole-dipole coupling ($n = 3$), and, in more ionized gases, quadratic Stark effects ($n = 4$). In weakly ionized atmospheric-pressure discharges like the one in this work, van der Waals and resonance broadening dominate. All of these mechanisms result in a Lorentzian line shape, which is why Lorentzian fitting is used throughout the spectral analysis [32].

Besides pressure broadening, two smaller mechanisms also contribute to the total line shape: **natural broadening** and **Doppler broadening**.

**Natural broadening** This effect results from the finite lifetime of the excited state, which creates a small uncertainty in its energy. It follows directly from the Heisenberg uncertainty principle and leads to a very narrow intrinsic line width [30].

**Doppler broadening** This type of broadening is caused by the random thermal motion of atoms or molecules, which shifts the wavelength of the absorbed light. It produces a Gaussian-shaped profile and is stronger for lighter species such as helium. At room temperature and atmospheric pressure, Doppler broadening is typically about one order of magnitude smaller than pressure broadening [5, 24].

## The fitting function

In principle, the total line profile is a Voigt function, representing the convolution of a Lorentzian. However, for this work, the Gaussian contribution is negligible. Therefore, the fitting has a pure Lorentzian profile. The formula for the helium fit, taken from [10], is a superposition of two Lorentzian functions with a spacing of 2.67 GHz and a relative signal strength of 0.6 [26]:

$$y(x) = y_0 + \frac{2aw}{\pi} \cdot \left( \frac{1}{4(x - x_0)^2 + w^2} + 0.6 \cdot \frac{1}{4(x - x_0 + 2.67)^2 + w^2} \right) \tag{2.14}$$

Argon fit is a single component Lorentzian without superposition:

$$y(x) = y_0 + \frac{2aw}{\pi} \cdot \frac{1}{4(x - x_0)^2 + w^2} \tag{2.15}$$

The variables in the Lorentzian fitting equations (Equations 2.14 and 2.15) are defined as follows:

$y(x)$ : The measured absorption signal at frequency (or wavelength) $x$.
$y_0$ : The background intensity in the absence of absorption.
$a$ : The area under the Lorentzian curve.
$w$ : The full Width at Half Maximum (FWHM) of the Lorentzian line profile.
$x$ : The frequency (or position on the detector) at which the measurement is taken.
$x_0$ : The center frequency (or wavelength) of the absorption line.

The parameter $a$ represents the integrated absorption and correspond to the left-hand side of 2.11.

# 3 Experimental Setup and Calibration

In this section, the experimental setup will be described in detail. As already mentioned in the introduction, a similar setup was used for a previous work [10], which serves as the main reference for writing this section. Further details, including the specific equipment used (such as device names and types), can be found there.

A simplified diagram of the setup is shown in Figure 3.1.

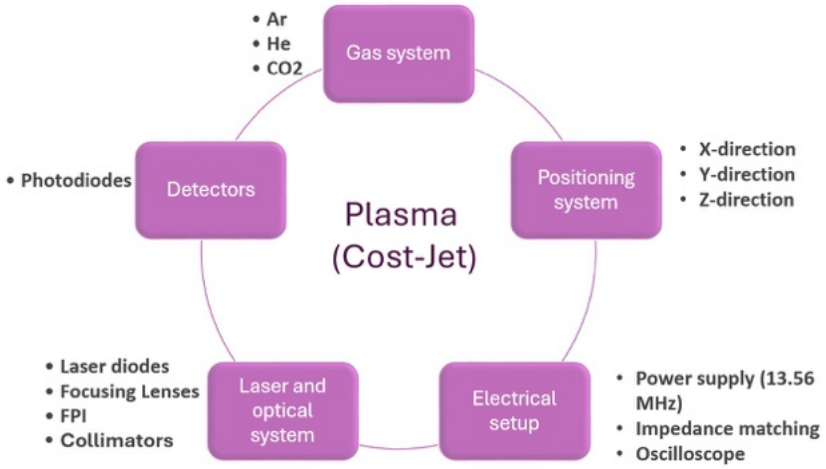


Figure 3.1: Block diagram of the setup

## 3.1 Plasma Source

As mentioned in the fundamentals section, the COST-Jet is the source of the plasma. Figure 3.2 presents a detailed schematic of the constituent components of the COST-Jet. It is a capacitively coupled, low-temperature RF plasma source that was developed in the COST Action MP1101. The discharge forms between two parallel electrodes, where one is grounded and the other is driven at 13.56 MHz. Together, the electrodes cover a cross-sectional area of 1 $mm^2$. A quartz window surrounds the discharge channel and gives very good optical access, which makes the setup well suited for TDLAS measurements. The voltage is controlled by an LC resonant circuit that works as a matching box. The plasma power supply is externally connected to the housing [11].

To determine the power dissipated in the plasma, an oscilloscope was connected to the current and voltage probes within the system. The voltage $U$ corresponds to the potential between the electrodes.

Based on the known resistances, the current can be derived from the measured voltage. The internal resistance of the COST-Jet is $R_m = 4.7\,\Omega$ [11] and the cable resistance is $R_t = 50\,\Omega$:

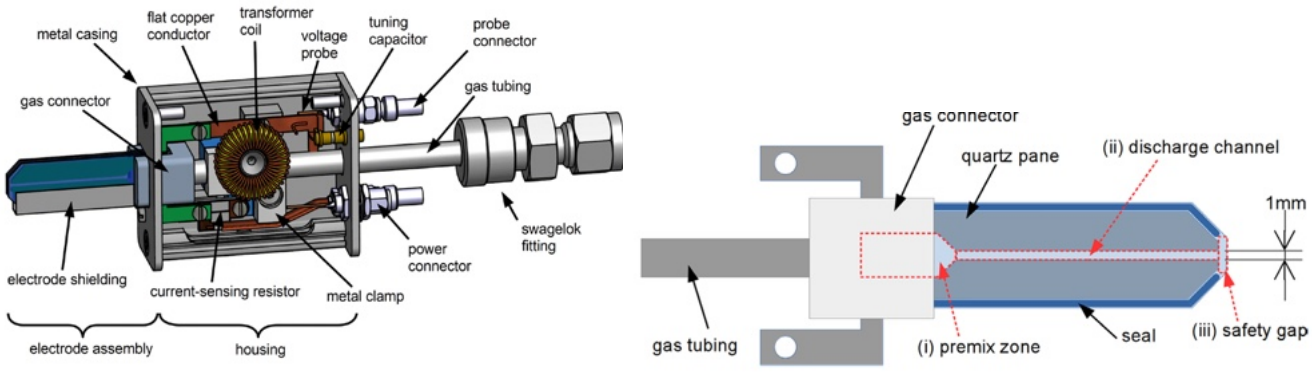


Figure 3.2: Sketches of the COST-Jet plasma source: (a) complete assembly with head, housing, and adapter; (b) detailed view of the jet head [11].

$$I = \frac{UR_m + UR_t}{R_m R_t} \tag{3.1}$$

The power P was calculated using the phase shift method. This method is described in [33], coordinated with the COST Power Monitor [34]:

$$P = U \cdot I \cdot \cos(\phi) \tag{3.2}$$

where $\phi$ is the phase difference between voltage and current [33].

The measurement of metastable densities using the COST-Jet as a plasma source offers several advantages. Its geometry is well defined, so experiments can be repeated under the same conditions. The jet also has a low gas temperature and a high electron density, which help excite atoms into metastable states more efficiently. In addition, $CO_2$ can be added in a controlled way, making it possible to study quenching and collisional energy transfer step by step [11].

## 3.2 Gas Supply System

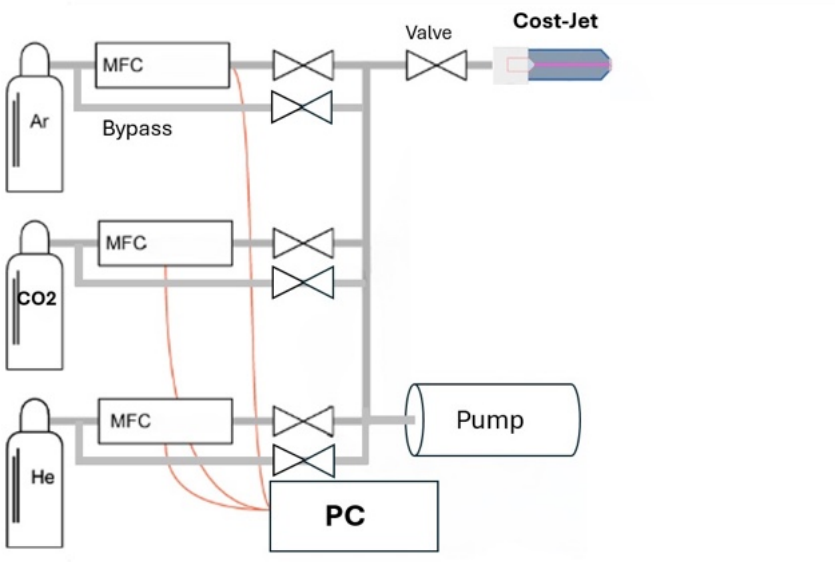


Figure 3.3: Gas supply system with three MFCs for Ar, $CO_2$, and He, including bypass lines, PC control, and the final valve leading to the COST-Jet.

The gas system used in this experiment is shown schematically in Figure 3.3. The helium, argon and $CO_2$ gases used are of high purity (99.999%).

The total feed gas flow (consisting of argon and helium) is set to 1,000 standard cubic centimeters per minute (sccm), with carbon dioxide ($CO_2$) added as an admixture to this base flow. The gas flow is regulated using three mass flow controllers (MFCs), all of which are operated via the LabVIEW program. The main gas line allows for a maximum flow of 2,000 sccm, the admixture line is limited to 500 sccm, and a third line is restricted to 20 sccm. The flow rates can be adjusted with a precision of 1% of the maximum flow.

Bypasses are installed around each mass flow controller to facilitate the purging of the gas lines. After the mass flow controllers and bypass lines, the valves are installed to regulate the pressure and control the direction of the gas flow. The entire setup, including the plasma jet, is connected through stainless steel tubing. A valve is placed directly behind the jet to prevent atmospheric air from entering the gas lines when the system is not in operation.

## 3.3 The Laser and Optical System

To study the metastable atoms in the plasma, a special laser and optical setup was built. It is based on tunable diode laser absorption spectroscopy (TDLAS). The system is fully operated through the LabVIEW program and is shown schematically in Figure 3.4.

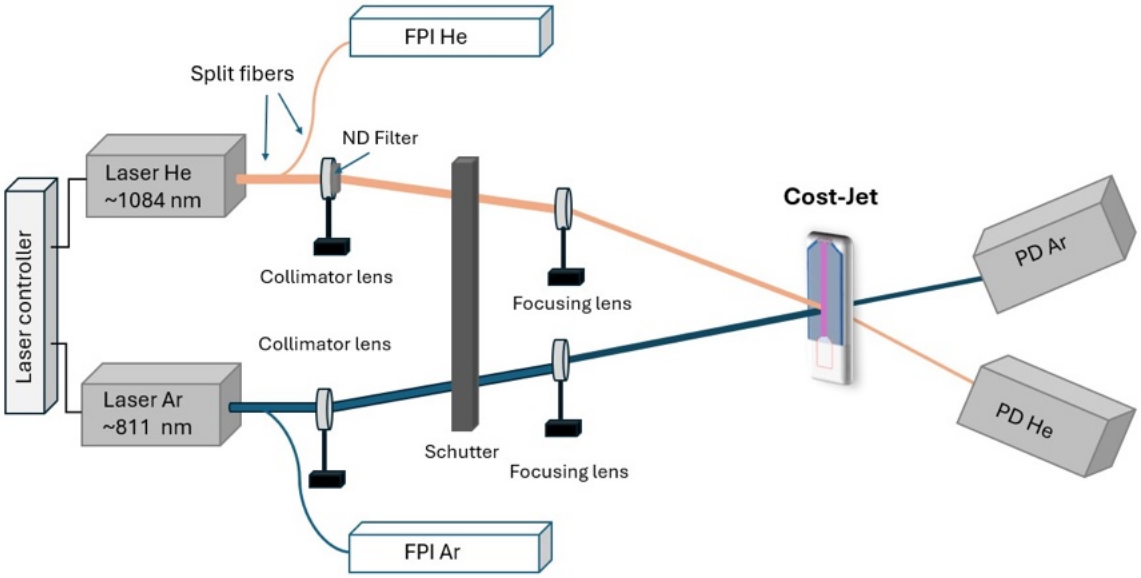


Figure 3.4: Optical layout for the TDLAS setup. The He (1084 nm) and Ar (811 nm) lasers are collimated, passed through the shutter, and focused through the COST jet, with part of each beam sent to the FPI for frequency calibration and the transmitted light detected by the photodiodes.

The schematic in Figure 3.4 provides an overview of the optical layout used in this work. Two diode lasers, one for helium and one for argon, are directed through their respective optical paths toward the plasma jet. Each beam passes through a collimation section and a focusing stage before entering the discharge region. A Fabry–Pérot interferometer (FPI) is placed in each beam path for frequency calibration. After passing through the plasma channel, the transmitted light is detected by two photodiodes placed behind the jet. A shutter is included in the optical path to block the beams when required. The figure illustrates the relative arrangement of the optical elements and the general beam geometry used during the measurements.

## 3.4 Positioning System

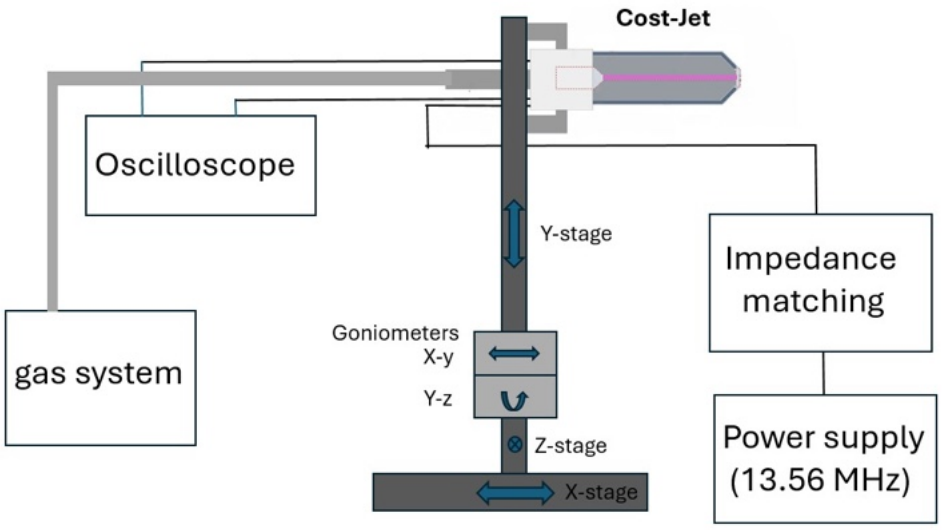


Figure 3.5: Positioning system of the COST-Jet with motorized x-, y-, and z-stages and goniometers for alignment, including the connections to the gas system, oscilloscope, impedance matching, and RF power supply.

The COST-Jet is mounted on a motorized translation stage that enables precise movement of the plasma source in all three spatial directions. The complete positioning system is illustrated in Figure 3.5. The system allows adjustments along the X, Y, and Z axes in micrometer-scale steps. Each direction has a total movement range of 100 mm. Movement is controlled by three stepper motors, each operated via the LabVIEW interface with sub-micrometer accuracy (better than 0.3 µm). The Z-axis runs parallel to the laser beam path. Changes in this direction influence the divergence of the beam and the focal overlap with the plasma channel as they alter the relative position between the lenses and the jet. The Y-axis corresponds to the vertical motion perpendicular to the lasers. The X-axis enables horizontal adjustments, also perpendicular to the beam direction. The system also includes two goniometers located beneath the plasma source. These allow for fine-tuning of the jet's angular position in both the x–y and y–z planes to ensure that the maximum of the laser beam is passing through the plasma gap. A fourth motorized stage is positioned between the collimating and focusing lenses. This stage is used to hold the shutter that can block the laser beam path when needed.

## 3.5 Optical Components and Beam Conditioning

### 3.5.1 Laser Diodes and Optical Configuration

Two laser diodes are used for the setup. Each diode is tuned to specific atomic transitions in helium and argon to selectively probe their respective metastable states. These diodes

are compact semiconductor sources composed of p-type and n-type layers.

Both laser diodes are connected to a laser controller, which regulates their operation and also functions as an oscilloscope to monitor output signals. The controller is also connected to the photodiodes to record their signals for later analysis.

Each laser diode is precisely aligned with a collimator, which reduces the natural divergence of the emitted beam, although the beam is not perfectly parallel due to imperfect fiber-collimator coupling. After that, the collimated beam passes through a focusing lens, which concentrates the light into the center of the discharge channel. For the helium laser, a lens with a focal length of 40 mm is used, while the argon beam is focused using a lens with a focal length of 90 mm. The minimum beam diameters at the focal point are approximately 130 µm for the helium beam and 75 µm for the argon beam, as determined during the calibration procedure (see Section 3.5.2).

A small fraction of each laser beam is simultaneously directed to a Fabry-Pérot interferometer (FPI), which is used to calibrate the frequency axis of the absorption spectra. Both beams are aligned such that their focal points coincide inside the discharge channel, ensuring that absorption is measured within the same plasma volume.

To avoid photodiode saturation due to the relatively high intensity of the helium laser, a neutral density filter (ND = 3) is placed directly behind its collimator lens.

The signals are detected by two photodiodes positioned behind the plasma jet. They will capture the transmitted laser light after it passes through the discharge channel. Photodiodes are ideal for detecting weak absorption signals in plasmas because of their high sensitivity, broad linear dynamic range, and fast response times (sub-nanosecond). They convert the intensity of the transmitted light into electrical signals, which makes it possible to observe the absorption in real time. Since the absorption is directly connected to the density of metastable species in the plasma, this method provides a reliable diagnostic tool for plasma analysis.

### 3.5.2 Calibration

This section describes the calibration procedures used to achieve accurate spatial alignment of the laser beams and a consistent interaction volume. It includes the determination of the beam width using the knife-edge technique and the optical alignment process with the COST-Jet.

#### Beam Width

The beam width was measured using the *knife-edge technique*. A schematic representation is shown in Figure 3.6. This widely used and accurate method determines the spatial profile of a laser beam, particularly under the assumption of a Gaussian intensity distribution.

In this method, a sharp edge is moved step by step across the laser beam, perpendicular to its propagation direction, while the transmitted intensity is recorded by a photodiode. As the edge gradually blocks or uncovers the beam, the recorded signal follows an S-shaped curve, which represents the integral of the Gaussian intensity profile and is typically described by an error function, as illustrated in Figure 3.7. Based on this analysis, a minimum beam width of approximately 65 µm was measured for the helium beam and around 38 µm for the argon beam, confirming the suitability of the optical configuration for spatially resolved TDLAS measurements.

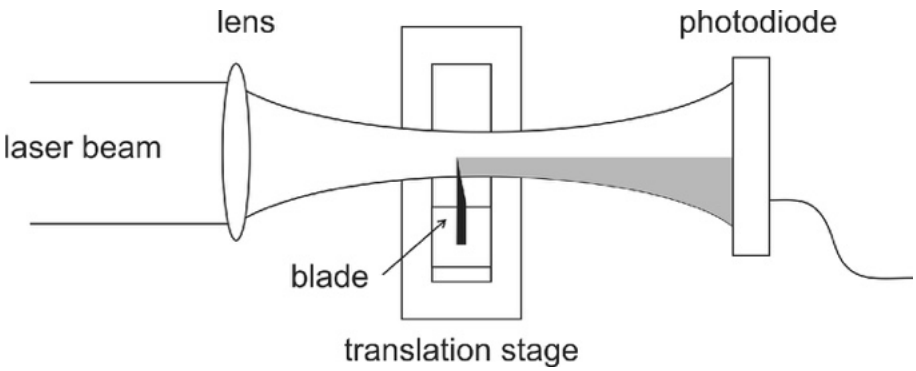


Figure 3.6: Simplified scheme for the measurement of laser beam width using the knife-edge technique [35].

The measured signal $P(x)$ as a function of knife-edge position $x$ is given by the following:

$$P(x) = \frac{P_0}{2}\left[1 + \mathrm{erf}\left(\frac{\sqrt{2}(x - x_0)}{w}\right)\right]$$

where:

- $P_0$ is the total beam power,
- $x_0$ is the beam center,
- $w$ is the $1/e^2$ beam width,
- and erf is the error function.

From the fitting of this equation, the beam width $w$ can be accurately extracted [35].

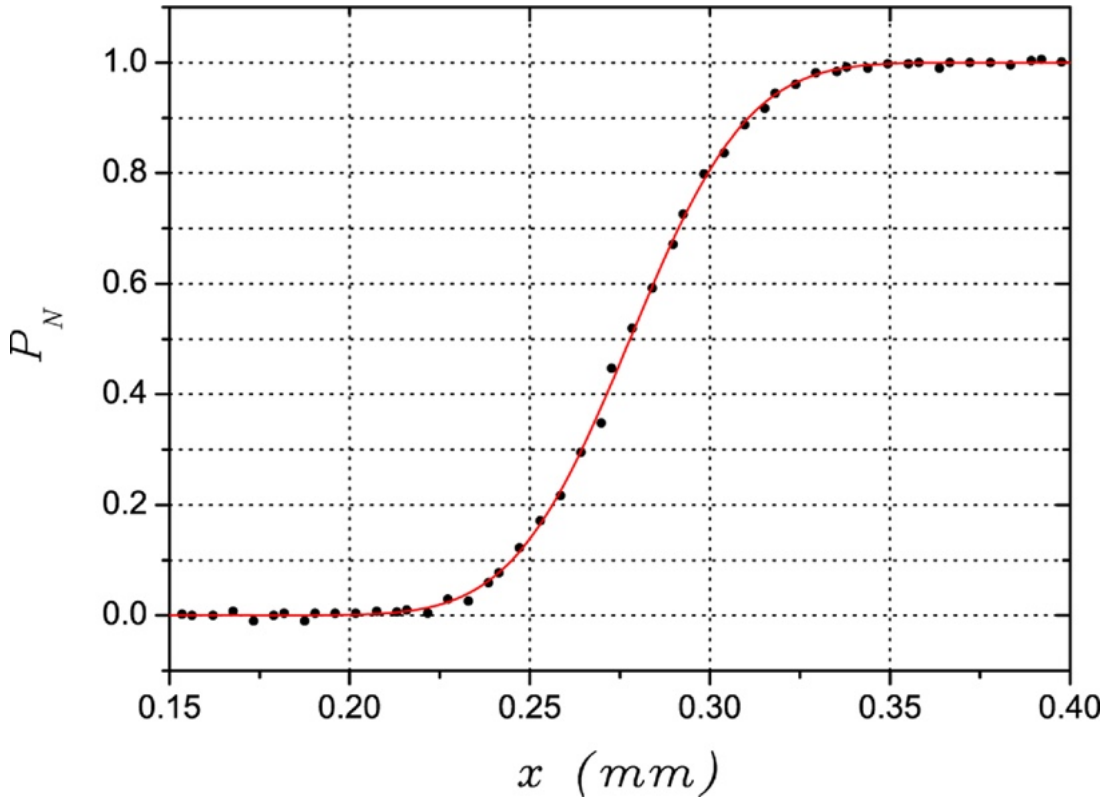


Figure 3.7: Example of the laser beam falloff function(black dotes) with the fitting(red line) in the knife-edge method from [35].

Figure 3.8 summarizes the measured beam widths for both lasers as a function of the distance to the focusing lens. From these measurements, minimum $1/e^2$ radii of approximately $w_{\mathrm{He}} = 64.7$ µm for the helium laser and $w_{\mathrm{Ar}} = 37.7$ µm for the argon laser were obtained. These values correspond to beam diameters of roughly 130 µm and 75 µm, respectively.

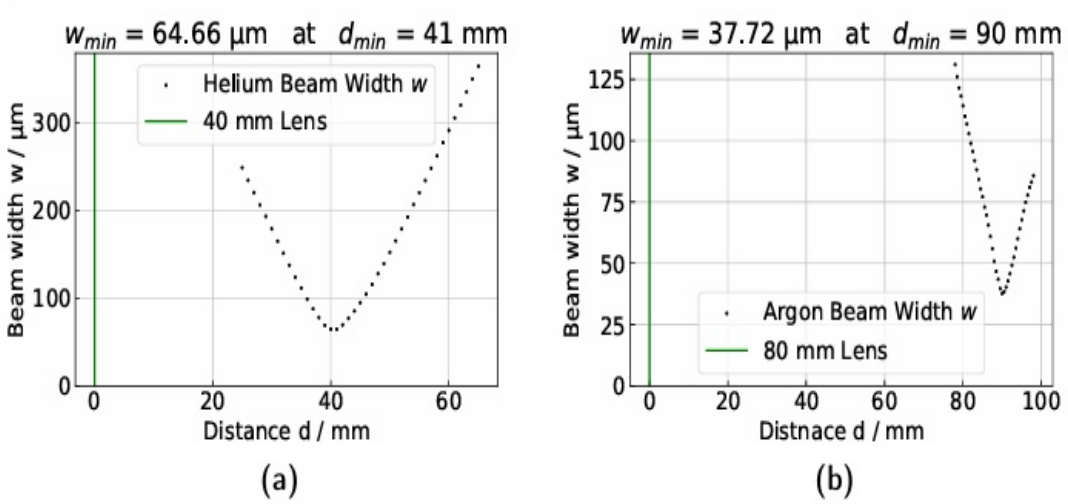


Figure 3.8: Beam width of the (a) helium laser with a 40 mm lens and (b) argon laser with an 80 mm lens as a function of the distance $d$ to the respective lens [10].

### Laser Alignment

For this work, precise overlap of the two laser beams is essential to ensure that the measurements are taken within the same plasma volume. However, achieving perfect spatial overlap was not feasible due to two key factors: first, the helium laser has a naturally wider beam diameter compared to the argon laser, and second, the optical setup introduces divergence in the beam path. The parallelization of the beam with external mirrors was intentionally avoided to keep the system simple and reduce the effort needed for alignment.

Each optical component (collimators, focusing lenses, and photodiodes) had to be manually adjusted to optimize signal strength and ensure beam intersection at the lenses' focal point. This proved to be very challenging and time-consuming. To confirm the vertical alignment, the plasma jet itself was used as a reference. The edges of the electrodes served as markers to check the position of the beam during fine adjustment. The positional tolerance had to be smaller than the 38 µm width of the argon beam (the narrower of the two lasers), especially in the X direction, as misalignment in this direction could result in sampling spatially distinct plasma regions. In the Y direction, errors were less critical, as vertical scans ultimately cover the same volume.

# 4 Measurements

This chapter presents the experimental measurements of the metastable argon density and its spatial distribution in the He/Ar/$CO_2$ plasma jet under varying power and gas mixture conditions. The results provide insight into how $CO_2$ influences the population of metastable atoms through quenching and energy transfer processes. The analysis of this measurements can help to better understand the dissociation of the $CO_2$. As described in the fundamentals, the absorption profile is based on the Beer-Lambert law. In the COST-Jet setup, the optical path length is 1 mm. However, because the laser beam crosses the plasma at a slight angle, the effective absorption path was experimentally found to be 1.089 mm [10]. This value was determined by a geometric estimation based on the distance between the jet and the focal lens, using Thales' theorem.

An example of the resulting absorption profile is presented in Figure 4.1. It shows the raw signal and its corresponding fit.

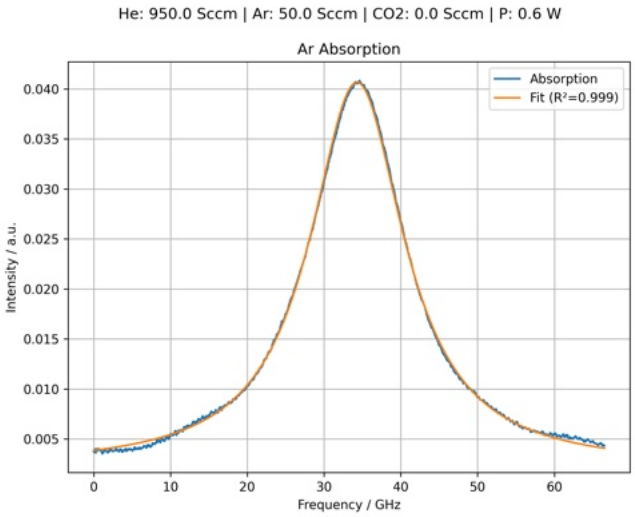


Figure 4.1: Example of an absorption line. The x-axis represent the frequency and the y.axis is the intensity.

## 4.1 Measurements Challenges and Potential Errors

The ignition of pure argon plasma in a COST-Jet has proven to be very challenging. This behavior is mainly explained by the physical properties of argon.

Compared to helium, argon has a lower ionization energy (15.76 eV vs. 24.59 eV). However, this does not always translate into easier plasma ignition. Argon actually requires a higher breakdown voltage at atmospheric pressure. In plasmas with high argon

admixture, electrons collide more frequently because argon atoms are heavier and more polarizable. This makes it harder for electrons to gain enough energy between collisions, reducing the efficiency in sustaining an avalanche.

The ignition process was further complicated by impurities within the gas lines. These included atmospheric air and residual water vapor. Even when the valve was positioned directly behind the jet, trace impurities could still diffuse from the jet nozzle whenever the gas flow was turned off. Even small amounts of oxygen ($O_2$) and water vapor ($H_2O$) can significantly change plasma properties by introducing new energy loss. These molecules are electronegative and can lower the free electron density through attachment, which reduces the chance of ionization and makes the discharge less stable [12, 27].

To eliminate impurities, the gas lines were purged by continuous vacuum pumping for 30 to 60 minutes before measurements. The pipes were gently heated (using a heat gun) during the pumping phase to speed up the desorption of water molecules adsorbed on the inner surfaces. After that, the system was further purged with pure argon at the highest possible flow rate (2000 sccm) for 15 to 30 minutes.

The initiation of the breakdown required the use of an external high-voltage ignition device, known as a Tesla coil igniter. This device generates a short but intense local electric field. This provides the initial seed electrons needed to start an electron avalanche in gases with higher breakdown thresholds. The device was held near the jet nozzle. Direct contact with the jet must be avoided, as it can trigger a power failure. Once the plasma was ignited, the external ignition was no longer needed, and the discharge could be maintained under standard RF excitation conditions.

It is important to note that we also had to start with a low flow of 500 sccm argon and then gradually increase the flow until we reached the desired 1000 sccm. This was necessary to avoid flow instabilities and to reduce back diffusion. At lower flow rates, back diffusion becomes stronger and can penetrate deeper into the discharge channel during startup.

When helium was used as the main feed gas, the plasma ignited without the need for an external trigger. Once a stable helium plasma was established, argon was gradually added to the gas mixture. The total gas flow was kept constant at 1000 sccm. Carbon dioxide was added on top of that. For high argon ratios (starting from 5% argon), heating and purging of the gas lines were necessary to improve the plasma stability.

The initial goal was to measure the density of metastable atoms, beginning with a pure helium plasma (0% argon) and gradually increasing the argon flow up to 100%. The same approach was intended with the addition of $CO_2$. However, in practice, this proved to be unfeasible. Most of the time, the plasma failed to ignite or was highly unstable.

Figure 4.2 illustrates the operational range of the experimental setup, where it was possible to obtain stable measurements.

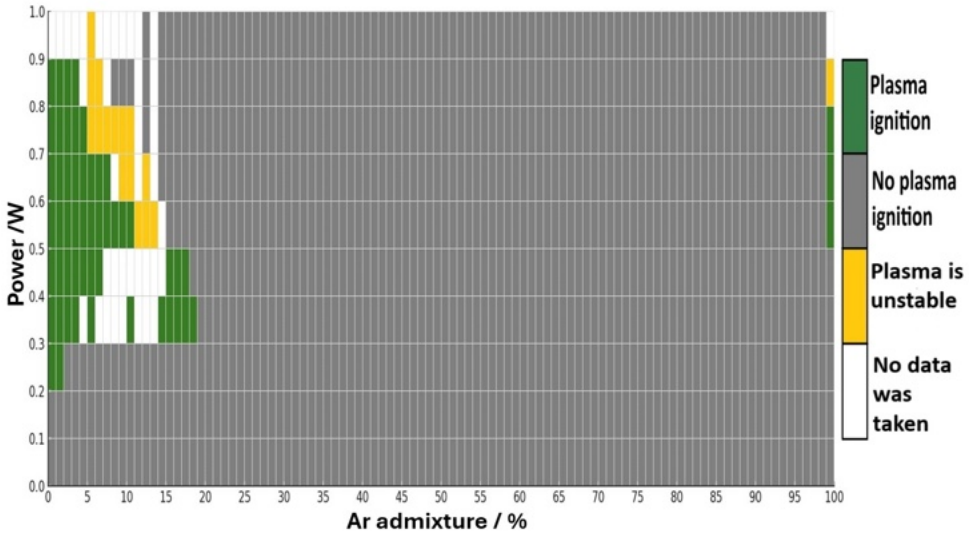


Figure 4.2: Map of plasma operational regimes without $CO_2$

The addition of 0.2 sccm $CO_2$ to the gas mixture had minimal impact on the operational regimes. In some cases, we explored increasing the $CO_2$ flow up to 0.8 sccm and we were still able to detect a signal. However, for most measurements, we used a fixed $CO_2$ flow of 0.2 sccm. At 100% argon, it was not possible to introduce any $CO_2$, as the plasma goes off immediately. This shows the destabilizing effect of $CO_2$ on the discharge.

The precision of the measurements was affected by several factors:

- The set of measurements required repeatedly switching the plasma on and off. Because the discharge did not reach thermal equilibrium before each data point was collected, small variations could occur in the metastable population between individual measurement cycles.
- Maintaining the same power level for a set of measurements was very challenging because adjustments had to be made manually. This led to an estimated power uncertainty of approximately $\pm 0.05$ W.
- Even after the careful purging of the gas lines, it is likely that small traces of impurities remained in the system. This may influence the quality of the measurements by affecting the absorption characteristics.
- To ensure the reliability of the absorption data, weak or noisy signals had to be filtered out. This was done using a Python script. The code evaluates the quality of the spectral fits based on the coefficient of determination ($R^2$). Any data with values of $R^2$ below 0.9 (where a perfect fit would correspond to $R^2 = 1$) were automatically excluded. However, a manual check was later performed to catch any unreliable fits that slipped through the automated process. This filtering also had the effect of removing low-density regions near the detection limit, which could lead to a slight tendency toward stronger signals.

The total error is difficult to determine precisely because of the combination of these systematic and statistical sources of uncertainty.

Due to time limitations, only one single vertical slice was measured for each parameter set. This slice was positioned at the midpoint of the discharge channel so that it was sufficiently far from the nozzle. This was done to avoid the influence of back diffusion from the surrounding atmosphere on the metastable density. The analysis of every vertical slice for each set of parameters would have been impractical, so a single representative density value was derived for each case and used as the basis for comparison. This value was calculated from the local maximum within the slice and its two neighboring points, but only if all three passed the quality checks already mentioned. This ensures that only reliable and consistent parts of the density profile were used in the analysis. If a neighboring data point did not pass the check, the algorithm automatically chooses the next highest valid density within the slice. In this way, the final density values remained consistent and physically meaningful in all measurements. The variation between the selected points was used to estimate the error bars shown in the plots. This offers a practical way to reflect local consistency without overwhelming the analysis with unreliable data. Importantly, this filtering approach tended to exclude low-density regions near the detection limit, where measurement uncertainty was highest.

## 4.2 Analysis of Ar Metastable Density with Gas Mixture Variations

In the previous work [10], it was observed that back diffusion of ambient air into the helium discharge brings in extra particles that affect the formation of helium metastable atoms. As argon mixture increased, the metastable density of the helium gradually decreased. At some point, it even fell below the detection limit. For example, at a power of 1.1 W, this happened when argon content was higher than 0.7%. In this work, the measurements start with adding 1% of argon. In this case, this reduction in helium metastable density was already observed for lower powers starting from 0.3 W. In all measurements performed for this study, no helium metastable density was detected. This can be explained due to the lower excitation energy threshold for argon compared to that for helium. As a result, argon is more likely to be excited by the electron energies commonly found in the plasma. Furthermore, when the gas mixture contains more argon, electrons collide with argon atoms more often. This further supports the formation of metastable argon atoms. The ionization rate of argon is also higher compared to that of helium due to its lower ionization energy. For this reason, argon atoms are more likely to be ionized by electron impacts. However, these advantages only apply up to a certain argon concentration. Once this limit is reached, other effects start to reduce the production of metastable atoms.

### 4.2.1 Argon variation with 0.0 and 0.2 sccm of $CO_2$

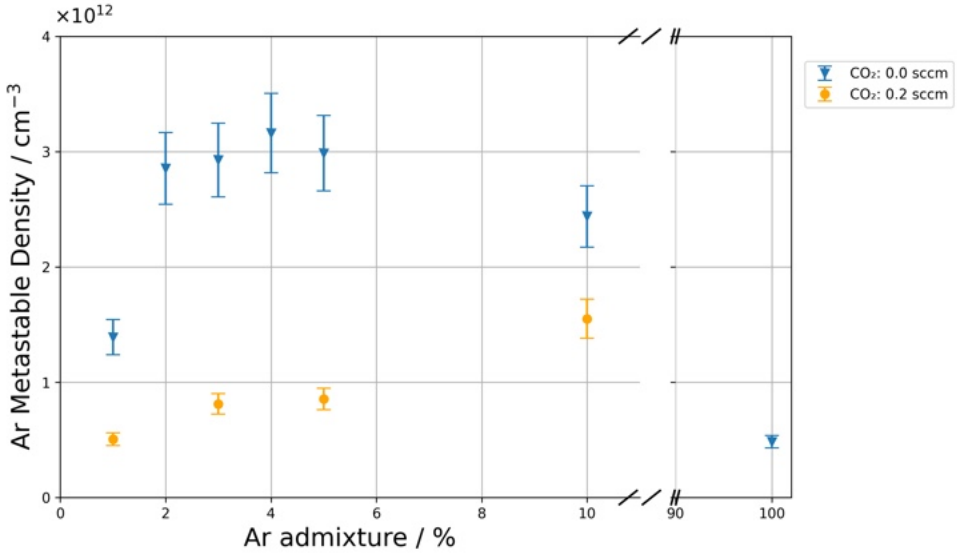


Figure 4.3: Ar metastable density against Ar admixture in percent at 0.5 W for $CO_2$ flows of 0.0 and 0.2 sccm.

At a power of 0.5 W, stable discharge conditions were achieved up to a maximum argon content of 10%, corresponding to 90% helium. Figure 4.3 shows the dependence of the argon metastable density on the argon admixture for two cases: without $CO_2$ (0.0 sccm, blue) and with a small $CO_2$ addition (0.2 sccm, orange).

Without $CO_2$, the Ar* density rises from approximately $1.4 \times 10^{12}\,\mathrm{cm}^{-3}$ at 1% Ar to a maximum of $3.2 \times 10^{12}\,\mathrm{cm}^{-3}$ around 4% admixture. Between 2–6% the density remains nearly constant, and then decreases to about $2.4 \times 10^{12}\,\mathrm{cm}^{-3}$ at 10%. In pure argon (100%), the metastable density drops to roughly $0.5 \times 10^{12}\,\mathrm{cm}^{-3}$.

This decrease at high argon amounts can likely be attributed to changes in the electron energy distribution. In a heavier gas, the average electron energy is expected to decrease because elastic collisions occur more frequently. This would lower the excitation rate into the Ar $(^3P_2)$ metastable level. Moreover, the argon-argon collisions may enhance three-body quenching and radiation-trapping effects, leading to shorter metastable lifetimes.

The addition of only 0.2 sccm $CO_2$ significantly reduces the metastable density across all admixtures. The $CO_2$ is a strong quencher of Ar* through both vibrational and electronic energy transfer channels. This significant decrease, even at low $CO_2$ levels, means that quenching is already a strong competitor to electron impact excitation at this power setting [1, 2].

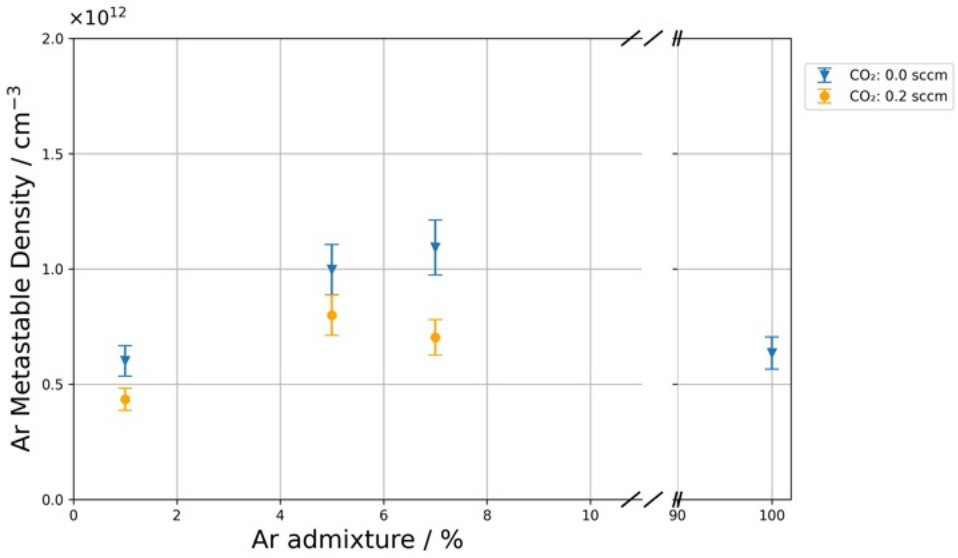


Figure 4.4: Ar metastable density against Ar admixture in percent at 0.6 W for $CO_2$ flows of 0.0 and 0.2 sccm.

At a slightly higher power of 0.6 W, the discharge remained stable up to about 7% argon admixture in helium. Figure 4.4 shows that, without $CO_2$, the metastable density increases from approximately $0.6 \times 10^{12}\,\mathrm{cm}^{-3}$ at 1% Ar to about $1.1 \times 10^{12}\,\mathrm{cm}^{-3}$ at 7% Ar. In pure argon, the metastable density again drops to roughly $0.6 \times 10^{12}\,\mathrm{cm}^{-3}$. This drop at 100% was also observed at 0.5 W and confirms that pure argon discharges are not favorable to maintain metastable under the given conditions.

This non monotonic trend is also seen in other atmospheric pressure plasma studies. Emmons *et al.* [36], who used numerical simulations to study metastable formation in atmospheric pressure dielectric barrier discharges (DBDs) with different Ar/He mixtures. Their model predicted that the $Ar(1s_5)$ metastable density increases with rising argon content, reaching a maximum at around 10-15% Ar, and then decreases again when the discharge contains more argon. While their discharge type (DBD) differs from our RF jet, their results show a similar qualitative trend, with our maximum appearing around 7% Ar. Their results also showed that the metastable density drops in pure argon. The physical explanation they provided is that at low Ar content, not enough argon is available to populate metastable levels, while at high Ar concentrations, more frequent Ar–Ar collisions lead to collisional quenching and lower electron energy. Although their discharge type and excitation method are different from our COST-Jet, their findings support the idea that an intermediate argon admixture gives the best conditions for Ar* formation under atmospheric pressure.

In our case, a similar trend was visible at different power levels. However, we cannot make any conclusion about the behavior at high argon admixtures, because in this range the plasma could not be ignited and no measurements were possible, as shown in Figure 4.2.

The increase in Ar* density at low argon admixtures can be explained as follows: When a small amount of argon is added to helium (around 1-7% Ar), the metastable density increases a lot. This is again related to the lower excitation and ionization thresholds of argon. At the same time, helium keeps the electrons energetic by supporting a higher reduced electric field (E/N), which helps with excitation. These conditions allow efficient excitation and also some ionization through metastable levels.

However, when the argon content becomes too high (closer to 100%), the situation changes. Since argon is now the main gas, the electron energy becomes lower because the reduced electric field decreases. Argon allows the discharge to run at lower E/N values. This makes the electrons not energetic enough to excite metastable atoms as efficiently. Also, the chance of metastable quenching increases. This happens through two-body collisions between $Ar^*$ and ground state Ar atoms, forming $Ar_2^*$ excimers and removing $Ar^*$. This type of quenching grows even faster at higher argon densities because the rate depends on the square of the Ar density [12, 36].

In addition, the plasma itself becomes more narrow in pure argon, a process known as discharge constriction. In helium, the plasma tends to stay more diffuse. But in high-argon conditions, it often contracts into thin filaments. This reduces the overall plasma volume, so even if the local metastable density is still high, the total amount is lower [37, 38]. All these effects-the less energetic electrons, more quenching, and smaller plasma volume-can explain why we see a drop in metastable density at 100% argon.

Finally, the results show that adding 0.2 sccm of $CO_2$ to the feed gas reduces the argon metastable density at all argon admixtures. In every case, the $CO_2$ curve lies below the one without $CO_2$. This shows that even a small amount of $CO_2$ has a clear quenching effect. One reason is that $CO_2$ introduces extra energy-loss channels. Electrons in the plasma can excite the vibrational or electronic states of $CO_2$, or cause dissociation, instead of exciting argon atoms. In this way, $CO_2$ takes away part of the electron energy that would normally be used to form metastable atoms. Other studies have also reported a strong decrease in Ar* density when small amounts of $CO_2$ were added. In plasma models, the vibrational excitation of $CO_2$ is known to be one of the main electron energy sinks, which confirms that this energy is no longer available for argon excitation. On top of that, $CO_2$ can also directly quench Ar* through collisional deactivation or Penning like reactions [1, 2, 36].

In summary, adding the $CO_2$ lowers the Ar* population across the full range of Ar admixtures. This agrees with the idea that $CO_2$ removes electron energy through vibrational excitation and quenching. The trend we see in Figure 4.4 fits well with previous results in atmospheric pressure He/Ar plasmas, and supports the general picture that metastable formation is highest at intermediate Ar content, but is reduced again when an energy-absorbing gas like $CO_2$ is present.

## 4.3 Power Variation

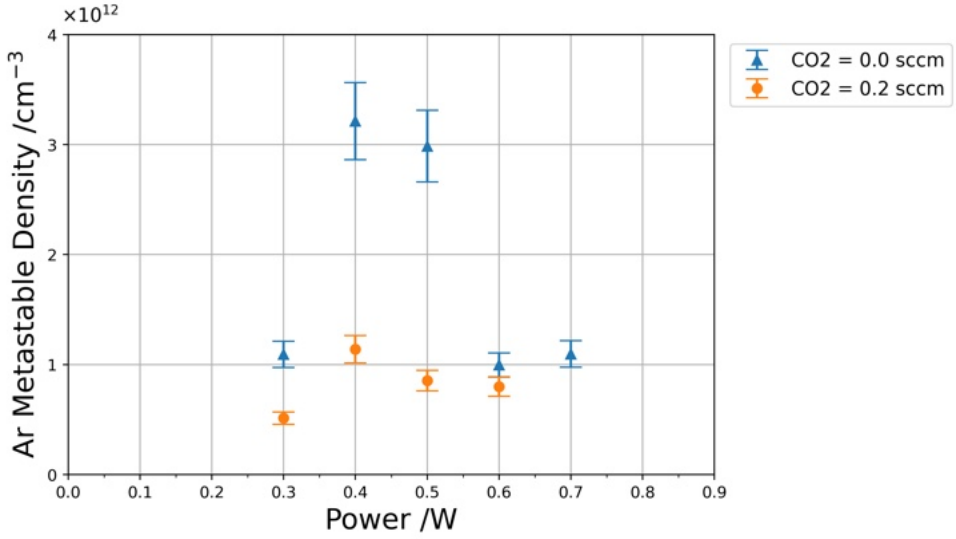


Figure 4.5: Ar metastable density as a function of applied power for an argon admixture of 5%, with and without 0.2 sccm $CO_2$.

The dependence of the argon metastable density on the applied power for a fixed 5% argon admixture is shown in Figure 4.5. For 0.0 sccm of $CO_2$, a non-linear trend is observed. The metastable density increases sharply between 0.3 W and 0.4 W, reaching a peak above $3 \times 10^{12}\,\mathrm{cm}^{-3}$. After this peak, it shows a strong decrease at 0.6 W and at 0.7 W.

In the previous work [10], the argon metastable density increased steadily with rising power and showed an almost linear trend with only small fluctuations across the whole power range. However, their measurements were done only for very low argon admixtures of less than 0.1%. In our measurements, this non monotonic behavior was unexpected, because in this low power range the metastable density is normally expected to increase almost linearly with the applied power. Nevertheless, the trend can be explained by changes in the discharge regime and in the electron energy distribution.

The initial increase indicates that, in this low to moderate power range, more electrons reach the ∼11.5 eV threshold required for exciting Ar atoms into the metastable $^3P_2$ state. Beyond ∼0.5 W, however, the behavior changes noticeably.

The spatial metastable profiles (more to this in the next section 4.3.1) clearly show a change in the discharge regime. Across the full power range from 0.3 W to 0.7 W, the profiles evolve from a nearly flat distribution in the center (0.3-0.4 W) into a structure with two maxima near the electrodes (0.6-0.7 W). This indicates a clear shift toward a sheath-influenced excitation regime. This observed redistribution explains the decrease in the measured Ar* density for the 0.6 and 0.7 W power. As the discharge becomes more sheath-affected, a larger fraction of electrons gains energy from the oscillating sheaths and exceeds the 15.8 eV ionization threshold, or drives stepwise ionization from existing metastable atoms (requiring only ∼4.1 eV). Both processes reduce the metastable population by diverting electrons away from the 11-13 eV range that is optimal for metastable excitation.

At higher powers, the additional RF input therefore does not lead to an increase in metastable density. Instead, the measured profiles confirm that excitation becomes con-

centrated near the electrode regions, the electron density increases, and the EEDF shifts probably toward energies where ionization dominates over excitation. These combined effects—the redistribution of excitation that we directly observe, the shift in the EEDF, and the increased losses through ionization—explain why the metastable density decreases despite the higher applied power.

Similar observations were also reported by Park et al. [39], who found that argon metastable densities in RF plasmas can peak at intermediate powers due to a shift in the electron energy distribution that favors ionization over excitation beyond a certain threshold.

At a $CO_2$ flow of 0.2 sccm, the metastable density is strongly reduced over the whole power range compared to the case without $CO_2$ (Figure 4.5). As discussed earlier, even a very small amount of $CO_2$ can efficiently quench argon metastable atoms through collisions, including vibrational excitation of $CO_2$. It also causes additional electron losses through attachment. Both processes lower the number of metastable atoms in the plasma. At the highest applied power of 0.4 W, no increase or recovery of the metastable density is observed. This shows that the quenching effect remains strong even at higher power. In summary, these results show that the balance between excitation and quenching is very sensitive in the presence of $CO_2$, and even a small amount shifts this balance clearly towards quenching.

### 4.3.1 Spatial Distribution of Ar Metastable Density

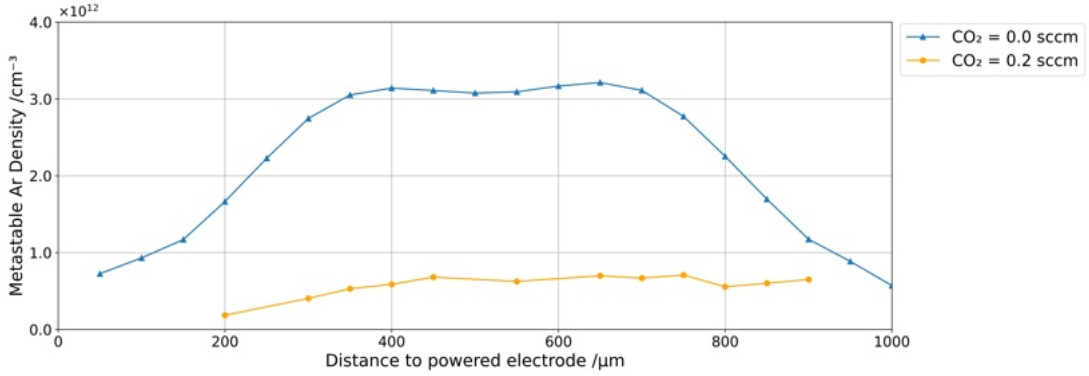


(a) 0.4 W

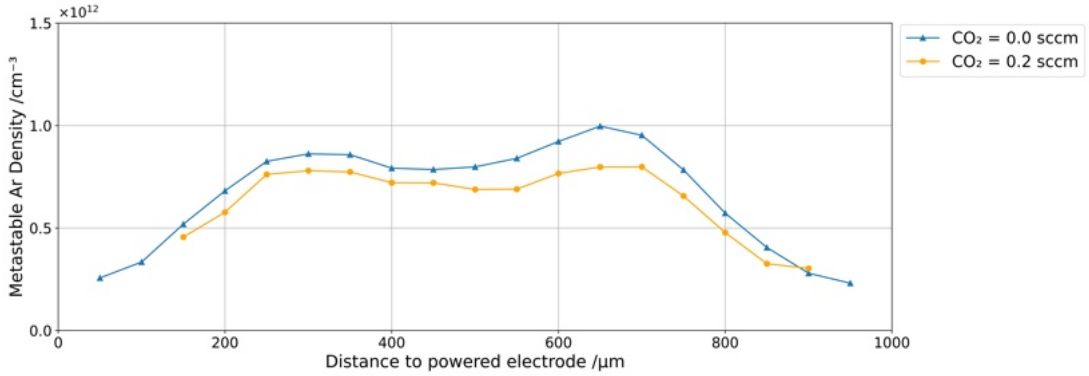


(b) 0.6 W

Figure 4.6: Spatial distribution of argon metastable density for an Ar admixture of 5% with $CO_2$ flow of 0.0 sccm and 0.2 sccm at 0.4 W and 0.6 W.

Figure 4.6 shows the spatially resolved argon metastable density for a 5% Ar admixture. It compares the cases with and without 0.2 sccm $CO_2$ at powers of 0.4 W and 0.6 W.

At 0.4 W, the density profile exhibits a broad central plateau between approximately 300 µm and 700 µm, with weak local maxima near both sides of the discharge region. This shape resembles an intermediate state between the typical Ω-mode and the Penning mode, where excitation is concentrated partly in the bulk and begins to extend toward the sheath regions. Similar central-flattened profiles were observed by Schulz-von der Gathen *et al.* [6, 7] for COST-Jets operating at moderate powers. The appearance of small peaks near the edges indicates that the sheath fields already play a role in exciting and sustaining metastable atoms even at this relatively low power.

The stronger excitation close to the electrodes can be attributed to increased electron heating in the oscillating sheath and to Penning ionization processes. These processes locally enhance electron production. Although the plasma still operates in an environment dominated by helium, the addition of 5% Ar is sufficient to make the discharge behave as an argon-dominated system. Since argon has a lower excitation threshold, it more easily undergoes electron-impact excitation and stepwise ionization.

At 0.6 W, two distinct maxima appear around 300 µm and 700 µm, while the central region becomes clearly depleted. This confirms the transition into the Penning mode, where the main excitation zones shift toward the electrode sheaths. The dip in the center is linked to a region with less electron density and energy. This shows that the formation of metastable atoms is now happening mostly in the areas adjacent to the sheath rather than in the plasma bulk.

Across both power levels, the addition of $CO_2$ lowers the metastable density at all positions. This also reinforces the previously observed strong quenching behavior. The reduction is nearly uniform across the discharge gap. This indicates that $CO_2$ quenching happens throughout the whole volume and is not limited to certain areas. The Penning mode becomes even more pronounced in the case of 100% argon, as shown in Figure 4.7. The central depletion in metastable density is deeper, and the two excitation maxima shift further toward the electrodes—one around 200 µm and the other near 750 µm. This indicates that the excitation and ionization processes are now strongly localized near the sheath edges.

In pure argon, the absence of helium reduces electron thermalization and increases the mean electron energy, especially in the sheath regions. As a result, energetic electrons more effectively populate the argon metastable level through direct excitation and stepwise ionization. Such spatially separated peaks have also been observed in other radio-frequency discharges dominated by argon, where sheath heating leads to stronger electric field oscillations and localized excitation [40, 41]. The enhanced stepwise ionization near the electrode zones further amplifies this localization. This produces the characteristic double peak structure of the Penning mode.

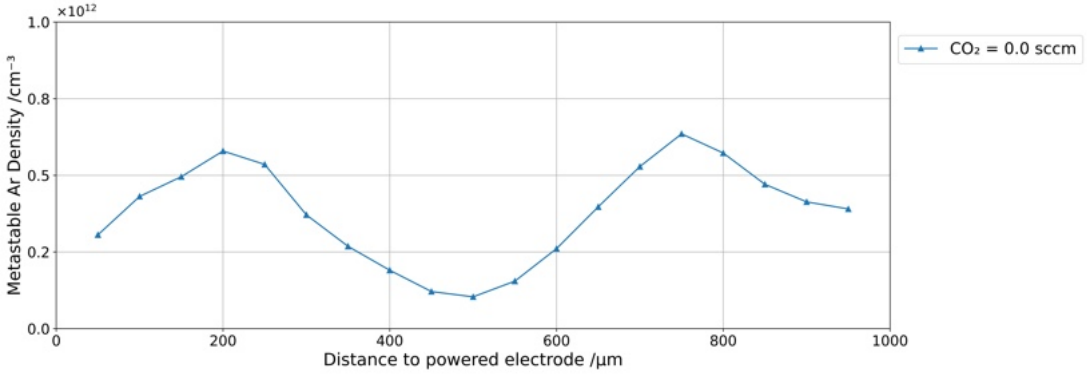


Figure 4.7: Spatial distribution of argon metastable density for an Ar admixture of 100% at 0.6 W.

A similar spatial pattern is expected when 0.2 sccm of $CO_2$ is introduced, but with considerably lower metastable densities. At 0.4 W, however, no distinct sheath-localized peaks are observed, and the discharge appears to remain in or close to the Ω-mode. The presence of $CO_2$ suppresses the transition toward the Penning mode by reducing the metastable population and thus weakening the Penning ionization feedback. The strong quenching ability of $CO_2$ not only reduces the overall metastable density but also changes the spatial energy distribution. As a result, the excitation zones no longer shift toward the sheath regions. Such suppression of Penning-related excitation by electronegative species has also been observed in Ar–$O_2$ and Ar–$CF_4$ mixtures [42, 43]. This supports the interpretation that $CO_2$ acts as an effective quencher that stabilizes the discharge in a more uniform, low-excitation regime.

### 4.3.2 Spatial Distribution with $CO_2$ Variation

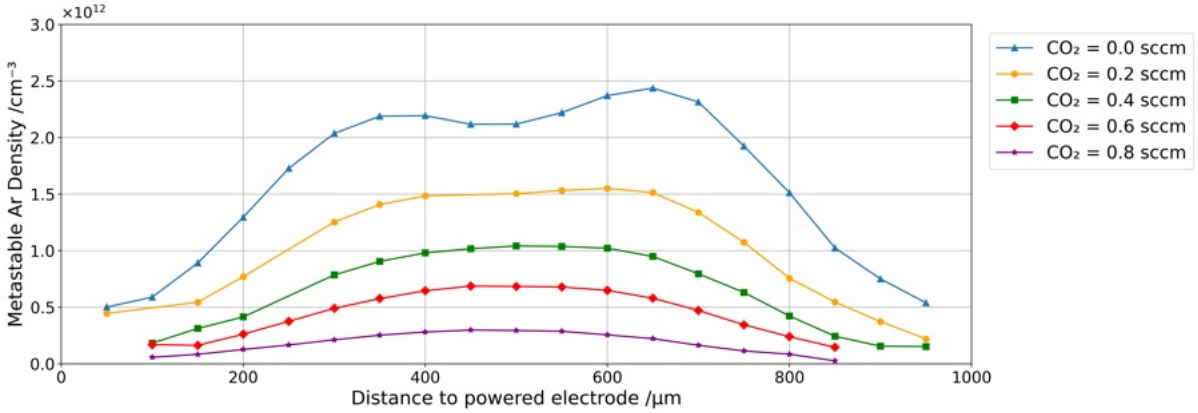


(a) Spatial distribution of Ar metastable density for 10% argon at 0.5 W with varying $CO_2$ flows.

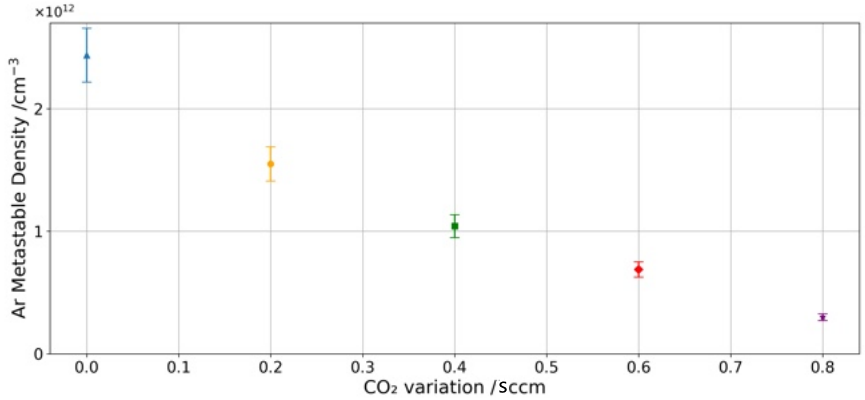


(b) Position of maximum metastable density for 10% argon at 0.5 W under different $CO_2$ admixtures.

Figure 4.8: Spatial distribution and peak positions of Ar metastable density for 10% Ar and various $CO_2$ flows at 0.5 W.

Figure 4.8 presents the spatially resolved metastable density for 10% Ar at 0.5 W as a function of increasing $CO_2$ admixture. For 0.0 sccm $CO_2$, the metastable density starts near $0.5 \times 10^{12}$ cm$^{-3}$ and rises steadily to a maximum of about $2.4 \times 10^{12}$ cm$^{-3}$ around 600 µm, followed by a gradual decrease toward the grounded electrode. The addition of $CO_2$ leads to a clear and progressive reduction of metastable density: approximately $1.5 \times 10^{12}$, $1.0 \times 10^{12}$, $0.7 \times 10^{12}$, and $0.3 \times 10^{12}$ cm$^{-3}$ for 0.2, 0.4, 0.6, and 0.8 sccm, respectively. This reinforces the earlier observations from the argon admixture and power variation results: The $CO_2$ acts as an effective quencher even at very low concentrations.

As the $CO_2$ admixture increases, the shape of the spatial profile also changes significantly. At 0.0 sccm, the distribution shows a pronounced double-peak structure, characteristic of Penning ($\gamma$-like) mode operation, where excitation and metastable formation are strongest near the sheath regions. With increasing $CO_2$, this double-peak gradually transforms into a smoother, centrally peaked profile, which is typical of the $\Omega$-mode.

This change shows that $CO_2$ does not just reduce the number of metastable atoms. It actually changes where the energy is deposited inside the plasma. Consequently, the plasma changes from a sheath-driven to a more homogeneous, bulk-dominated excitation

regime. In this regime, processes involving metastable atoms are strongly suppressed. Such behavior supports the general view that $CO_2$ addition stabilizes the discharge while simultaneously reducing the role of metastable atoms in energy transfer and chemical activation.

# 5 Conclusion

In this work, the spatially resolved densities of the Ar ($^3P_2$) metastable state in a radio-frequency (RF) atmospheric pressure He–Ar–$CO_2$ plasma jet were systematically investigated using tunable diode laser absorption spectroscopy (TDLAS). The study aimed to reveal how gas composition, applied power, and $CO_2$ admixture influence the generation, distribution, and quenching of metastable atoms, and how these processes affect the overall plasma energy balance.

One of the main experimental challenges was igniting and maintaining a stable plasma. This was particularly problematic at high argon concentrations (above about 7–10% Ar depending on the applied power). Therefore, each measurement required careful purging and flushing of the gas line. Another challenge was achieving a stable alignment of the laser beam across the discharge channel to enable spatially resolved absorption measurements.

The results show that, for the investigated gas mixtures, no helium metastable atoms were detectable. This observation is consistent with earlier studies that reported the disappearance of helium metastable atoms even at very low argon admixtures (0.07%). As a result, the focus of this study was placed exclusively on metastable argon atoms.

The accessible range of argon admixtures for stable operation was limited. Across all tested power levels, the ignition was completely impossible for argon admixtures between 18-99%. Measurements in pure argon were only possible for power levels between 0.5 and 0.8 W.

The addition of argon enhances the metastable density up to a certain concentration. After approximately 6–8% argon, the density begins to decrease, reaching the lowest values in pure argon discharges. This decline is attributed to a reduction in electron temperature and increased collisional quenching at higher argon contents.

The variation of metastable argon density with applied power follows a distinct trend. At lower powers ( 0.4 W), the density increases almost linearly as more electrons are available for excitation. The maximum density of over $3 \times 10^{12}\,\mathrm{cm}^{-3}$ was measured at 0.4 W for 5% argon. However, beyond this power ( 0.5 W), the metastable density drops sharply. This decrease is not only caused by enhanced loss channels such as ionization, but also by a change in the electron energy distribution. At higher power, the electron density increases and the EEDF shifts toward lower mean energies. As a result, fewer electrons populate the $\sim 11.5\,\mathrm{eV}$ range required to excite Ar atoms into the $^3P_2$ state. Increasing the power does not necessarily lead to higher metastable production. At higher power, more of the input energy is used to sustain the plasma and to drive ionization instead of excitation.

The spatially resolved measurements revealed that, at 0.4 W without $CO_2$, the metastable argon density peaks near the center but also exhibits two smaller maxima away from the axis. This distribution suggests a transition from Ohmic toward Penning ($\gamma$-like) mode,

where excitation and ionization predominantly occur near the sheath regions with higher electric fields. At 0.6 W, these edge peaks become more pronounced. This confirm the operation in the Penning mode. This double-peak structure indicates that energy deposition occurs mainly near the boundaries of the discharge channel.

The addition of even small amounts of $CO_2$ (0.2 sccm) resulted in a pronounced reduction of metastable density and a flattening of its spatial distribution. This indicates that $CO_2$ not only decreases the metastable population but also redistributes the local energy balance within the discharge. Increasing the $CO_2$ admixture at a constant power of 0.5 W led to a strong and continuous suppression of metastable density. The plasma simultaneously transitioned from a Penning-type double-peak profile to a more uniform, centrally peaked shape characteristic of Ohmic mode operation. This behavior shows that $CO_2$ influences not only metastable quenching but also the spatial distribution of excitation energy. This highlights its strong impact on energy transport mechanisms in atmospheric pressure plasma jets.

Metastable argon atoms possess sufficient internal energy to dissociate $CO_2$ through Penning-type reactions. Initially, this could explain the reduction in metastable density upon adding $CO_2$. However, the measured densities decrease sharply and immediately, even at very low $CO_2$ concentrations, without reaching saturation. This behavior points predominantly to physical quenching rather than chemical dissociation. Moreover, the transition from a double peaked to a smooth spatial profile supports this interpretation: $CO_2$ not only removes metastable atoms through inelastic collisions but also alters the plasma's mode of operation and spatial energy distribution. In summary, the results indicate that the apparent loss of metastable atoms in He–Ar–$CO_2$ plasma jets is mainly governed by quenching mechanisms rather than direct dissociative reactions with $CO_2$.

## 5.1 Limitations and Future Perspectives

One of the main limitations of this work was the restricted operational range of the plasma at high argon concentrations. In particular, the admixtures between 18% and 99% could not be stabilized at any of the applied power levels. As a result, measurements in this range could not be performed, which limits the possibility of identifying potential transition points between the Ohmic and Penning modes under changing admixture conditions.

The influence of $CO_2$ on the electron energy distribution was not measured directly and remains an open question. Since vibrational excitation and electron attachment can significantly affect the energy balance in the plasma, additional diagnostics such as optical emission spectroscopy (OES) or Langmuir probe measurements would help to better understand how $CO_2$ changes discharge conditions.

In future work, it would be useful to perform direct measurements of $CO_2$ dissociation products to confirm the role of metastable atoms in the conversion process. This could be done by combining TDLAS with mass spectrometry or infrared absorption techniques. It would also be interesting to extend the spatial resolution in the axial direction, especially to investigate whether the suppression of metastable by $CO_2$ also shifts the active zones in the plasma.

Finally, operating the plasma in different modes or excitation frequencies, or introducing pulsed operation, could provide further insight into how metastable-driven dissociation pathways behave under time-varying conditions.

# Bibliography


[1] R. Snoeckx and A. Bogaerts. Plasma technology – a novel solution for CO2 conversion? *Chemical Society Reviews*, 46(19):5805–5863, October 2017.

[2] A. Bogaerts and G. Centi. Plasma Technology for CO2 Conversion: A Personal Perspective on Prospects and Gaps. *Frontiers in Energy Research*, 8:111, July 2020.

[3] S. Renninger, M. Lambarth, and K. P. Birke. High efficiency CO2-splitting in atmospheric pressure glow discharge. *Journal of CO2 Utilization*, 42:101322, December 2020.

[4] A. Fridman. *Plasma Chemistry*. Cambridge University Press, Cambridge, online-ausg edition, 2008.

[5] K. Niemi, J. Waskoenig, N. Sadeghi, T. Gans, and D. O'Connell. The role of helium metastable states in radio-frequency driven helium–oxygen atmospheric pressure plasma jets: measurement and numerical simulation. *Plasma Sources Science and Technology*, 20(5):055005, October 2011.

[6] V. Schulz-von Der Gathen, V. Buck, T. Gans, N. Knake, K. Niemi, St. Reuter, L. Schaper, and J. Winter. Optical Diagnostics of Micro Discharge Jets. *Contributions to Plasma Physics*, 47(7):510–519, November 2007.

[7] V. Schulz-von Der Gathen, L. Schaper, N. Knake, S. Reuter, K. Niemi, T. Gans, and J. Winter. Spatially resolved diagnostics on a microscale atmospheric pressure plasma jet. *Journal of Physics D: Applied Physics*, 41(19):194004, October 2008.

[8] C. Stewig, S. Schüttler, T. Urbanietz, M. Böke, and A. Von Keudell. Excitation and dissociation of $CO_2$ heavily diluted in noble gas atmospheric pressure plasma. *Journal of Physics D: Applied Physics*, 53(12):125205, March 2020.

[9] L. D. Pietanza, G. Colonna, G. D'Ammando, A. Laricchiuta, and M. Capitelli. Vibrational excitation and dissociation mechanisms of $CO_2$ under non-equilibrium discharge and post-discharge conditions. *Plasma Sources Science and Technology*, 24(4):042002, July 2015.

[10] A. Schicke. Absorption measurements of the metastable atom density in an atmospheric pressure plasma. Master's thesis, Ruhr-Universität Bochum, Faculty of Physics and Astronomy, Bochum, 2024.

[11] J. Golda, J. Held, B. Redeker, M. Konkowski, P. Beijer, A. Sobota, G. Kroesen, N. Braithwaite, S. Reuter, M. M. Turner, T. Gans, D. O'Connell, and V. Schulz-von der Gathen. Concepts and characteristics of the "COST Reference Microplasma Jet". *Journal of Physics D: Applied Physics*, 49(8), January 2016.

[12] Y. P. Raizer. *Gas Discharge Physics*. Springer Berlin Heidelberg, Berlin, Heidelberg, 1991.

[13] K. T. A. L. Burm. Calculation of the Townsend Discharge Coefficients and the Paschen Curve Coefficients. *Contributions to Plasma Physics*, 47(3):177–182, May 2007.

[14] M. A. Lieberman and A. J. Lichtenberg. *Principles of Plasma Discharges and Materials Processing*. Wiley, 1 edition, April 2005.

[15] S. Spiekermeier. *Transient metastable dynamics in atmospheric pressure microplasma jets*. PhD thesis, Ruhr university Bochum, February 2016.

[16] E. Marode. The mechanism of spark breakdown in air at atmospheric pressure between a positive point and a plane. I. Experimental: Nature of the streamer track. *Journal of Applied Physics*, 46(5):2005–2015, May 1975.

[17] K. Woodruff, J. Baeza-Rubio, D. Huerta, B.J.P. Jones, A.D. McDonald, L. Norman, D.R. Nygren, C. Adams, V. Álvarez, L. Arazi, I.J. Arnquist, C.D.R Azevedo, K. Bailey, F. Ballester, J.M. Benlloch-Rodríguez, F.I.G.M. Borges, N.K. Byrnes, S. Cárcel, J.V. Carrión, S. Cebrián, E. Church, C.A.N. Conde, T. Contreras, A.A. Denisenko, G. Díaz, J. Díaz, M. Diesburg, J. Escada, R. Esteve, R. Felkai, A.F.M. Fernandes, L.M.P. Fernandes, P. Ferrario, A.L. Ferreira, F.W. Foss Jr., E.D.C. Freitas, J. Generowicz, A. Goldschmidt, D. González-Díaz, J.J. Gómez-Cadenas, S. Ghosh, R. Guenette, R.M. Gutiérrez, J. Haefner, K. Hafidi, J. Hauptman, C.A.O. Henriques, J.A. Hernando Morata, P. Herrero, V. Herrero, S. Johnston, M. Kekic, L. Labarga, A. Laing, P. Lebrun, N. López-March, M. Losada, R.D.P. Mano, J. Martín-Albo, A. Martínez, G. Martínez-Lema, F. Monrabal, C.M.B. Monteiro, F.J. Mora, J. Muñoz Vidal, P. Novella, B. Palmeiro, A. Para, J. Pérez, M. Querol, J. Renner, J. Repond, S. Riordan, L. Ripoll, Y. Rodriguez Garcia, J. Rodríguez, L. Rogers, B. Romeo, C. Romo-Luque, F.P. Santos, J.M.F. Dos Santos, A. Simón, C. Sofka, M. Sorel, T. Stiegler, P. Thapa, J.F. Toledo, J. Torrent, A. Usón, J.F.C.A. Veloso, R. Webb, R. Weiss-Babai, J.T. White, and N. Yahlali. Radio frequency and DC high voltage breakdown of high pressure helium, argon, and xenon. *Journal of Instrumentation*, 15(04):P04022–P04022, April 2020.

[18] R. Rahul, O. Stan, A. Rahman, E. Littlefield, K. Hoshimiya, A. P. Yalin, A. Sharma, A. Pruden, C. A. Moore, Z. Yu, and G. J. Collins. Optical and RF electrical characteristics of atmospheric pressure open-air hollow slot microplasmas and application to bacterial inactivation. *Journal of Physics D: Applied Physics*, 38(11):1750–1759, June 2005.

[19] D. W. Liu, F. Iza, and M. G. Kong. Electron heating in radio-frequency capacitively coupled atmospheric-pressure plasmas. *Applied Physics Letters*, 93(26):261503, December 2008.

[20] T. Hemke, D. Eremin, T. Mussenbrock, A. Derzsi, Z. Donkó, K. Dittmann, J. Meichsner, and J. Schulze. Ionization by bulk heating of electrons in capacitive radio frequency atmospheric pressure microplasmas. *Plasma Sources Science and Technology*, 22(1):015012, December 2012.

[21] D. Schröder, S. Burhenn, T. De Los Arcos, and V. Schulz-von Der Gathen. Characteristics of a propagating, self-pulsing, constricted 'gamma-mode-like' discharge. *Journal of Physics D: Applied Physics*, 48(5):055206, February 2015.

[22] F. Massines, A. Rabehi, P. Decomps, R. Ben Gadri, Pierre Ségur, and Christian Mayoux. Experimental and theoretical study of a glow discharge at atmospheric pressure controlled by dielectric barrier. *Journal of Applied Physics*, 83(6):2950–2957, March 1998.

[23] C. Gerry and P. Knight. *Introductory Quantum Optics*. Cambridge University Press, 1 edition, October 2004.

[24] B. Niermann, M. Böke, N. Sadeghi, and J. Winter. Space resolved density measurements of argon and helium metastable atoms in radio-frequency generated He-Ar micro-plasmas. *The European Physical Journal D*, 60(3):489–495, December 2010.

[25] D. P. Lymberopoulos and D. J. Economou. Fluid simulations of glow discharges: Effect of metastable atoms in argon. *Journal of Applied Physics*, 73(8):3668–3679, April 1993.

[26] National Institute of Standards and Technology (NIST). Atomic spectra database lines form, 2023. Accessed: Dec. 2023.

[27] B. Niermann. *The role of metastable atoms in radio-frequency micro-plasma jet discharges operated at atmospheric pressure*. doctoralthesis, Ruhr-Universität Bochum, Universitätsbibliothek, 2012.

[28] M. Kassayová, L. Uvarova, P. Dohnal, Š. Roučka, R. Plašil, and J. Glosík. Penning ionization of $N_2$ by helium metastable atoms. In *WDS'23 Proceedings of Contributed Papers – Physics*. MATFYZPRESS, 2023.

[29] N. Sadeghi. 6. Molecular Spectroscopy Techniques Applied for Processing Plasma Diagnostics. *Journal of Plasma and Fusion Research*, 80(9):767–776, 2004.

[30] W. Demtröder. *Laser Spektroskopie 1*. Springer Berlin Heidelberg, Berlin, Heidelberg, 2014.

[31] H. R. Griem. *Principles of Plasma Spectroscopy*. Cambridge Monographs on Plasma Physics. Cambridge University Press, Cambridge, 1997.

[32] A. Corney. *Atomic and Laser Spectroscopy*. Oxford University Press, Oxford, 2006.

[33] V. A. Godyak and R. B. Piejak. In situ simultaneous radio frequency discharge power measurements. *Journal of Vacuum Science & Technology A: Vacuum, Surfaces, and Films*, 8(5):3833–3837, September 1990.

[34] J. Held. mimurrayy/cost-power-monitor, 2023. Accessed: 2023-12. Original-date: 2018-07-04T15:42:46Z.

[35] M. A. de Araújo, R. Silva, E. de Lima, D. P. Pereira, and P. C. de Oliveira. Measurement of gaussian laser beam radius using the knife-edge technique: improvement on data analysis. *Appl. Opt.*, 48(2):393–396, Jan 2009.

[36] D. J. Emmons, D. E. Weeks, B. Eshel, and G. P. Perram. Metastable Ar(1s5) density dependence on pressure and argon-helium mixture in a high pressure radio frequency dielectric barrier discharge. *Journal of Applied Physics*, 123(4):043304, January 2018.

[37] J. Golda, J. Held, and V. Schulz-von Der Gathen. Comparison of electron heating and energy loss mechanisms in an RF plasma jet operated in argon and helium. *Plasma Sources Science and Technology*, 29(2):025014, February 2020.

[38] J. Li, B. Lei, J. Wang, B. Xu, S. Ran, Y. Wang, T. Zhang, J. Tang, W. Zhao, and Y. Duan. Atmospheric diffuse plasma jet formation from positive-pseudo-streamer and negative pulseless glow discharges. *Communications Physics*, 4(1):64, March 2021.

[39] M. Park, H. Chang, S. You, J. Kim, D. Seong, and Y. Shin. A simple analysis on the abnormal behavior of the argon metastable density in an inductively coupled Ar plasma. *Thin Solid Films*, 518(22):6694–6699, September 2010.

[40] Z. Donkó, P. Hartmann, I. Korolov, D. Schulenberg, S. Rohr, S. Rauf, and J. Schulze. Metastable argon atom kinetics in a low-pressure capacitively coupled radio frequency discharge. *Plasma Sources Science and Technology*, 32(6):065002, June 2023.

[41] L. Zhao, Y. Liu, and T. Samir. Numerical study on discharge characteristics influenced by secondary electron emission in capacitive RF argon glow discharges by fluid modeling. *Chinese Physics B*, 27(2):025201, February 2018.

[42] M. Vass, S. Wilczek, J. Schulze, and Z. Donkó. Electron power absorption in micro atmospheric pressure plasma jets driven by tailored voltage waveforms in $He/N_2$. *Plasma Sources Science and Technology*, 30(10):105010, October 2021.

[43] S. Rauf and M. J. Kushner. Argon metastable densities in radio frequency Ar, Ar/O2 and Ar/CF4 electrical discharges. *Journal of Applied Physics*, 82(6):2805–2813, September 1997.

Table : Declaration of AI Tools

| **AI Tool*** | **Type of Use*** | **Affected Sections*** | **Notes**** |
|---|---|---|---|
| **DeepL Write** | DeepL Write helped me to make my sentences clearer and in a better academic style. | This was used mainly in the abstract, Heating Mechanism and Optical Components and Beam Conditioning and Line Broadening in Absorption Spectroscopy | |
| **ChatGPT** | ChatGPT helped me understand plasma physics ideas in a simple way (metastables, EEDF, quenching, sheath and bulk, excitation, line broadening). It helped write most of the Python code (about 90%) to create the figures. It also supported me in Overleaf by helping with equations, fixing errors, and solving LaTeX problems. It also supported me when going through the references by helping me understand them and find the key points. It helped improve the clarity and polish of several sentences, especially in the section "Characterization of Plasmas". It also supported me when going through the references by helping me understand them and find the key points. It also translated the whole abstract into German. | Whole thesis (theory, coding, Overleaf) | Used for explanation, coding and translation. |
| **Manus** | Manus helped me find scientific papers related to my topic. It also gave general feedback on the thesis at the end | Multiple chapters during writing | Used for literature search and chapter feedback. |
| **DeepSeek** | DeepSeek helped me by find better synonyms for example i ask it, "how can i replace this word in the sentence?" It also checked if my sentences were grammatically correct and physically correct. | General writing across the thesis | Used for language improvement and correctness. |